In vivo discovery of RNA proximal proteins in human cells via proximity-dependent biotinylation

Xianzhi Lin[1, 2] *, Marcos A. S. Fonseca[1, 2], Rosario I. Corona [1, 2], Kate Lawrenson[1, 2, 3] *

[1]Women's Cancer Research Program at Samuel Oschin Comprehensive Cancer Institute, Cedars-Sinai Medical Center, Los Angeles, CA, USA.

[2]Division of Gynecologic Oncology, Department of Obstetrics and Gynecology, Cedars-Sinai Medical Center, Los Angeles, CA, USA.

[3]Center for Bioinformatics and Functional Genomics, Samuel Oschin Comprehensive Cancer Institute, Cedars-Sinai Medical Center, Los Angeles, CA, USA.

*Correspondence: xianzhi.lin@cshs.org (X.L.) or kate.lawrenson@cshs.org (K.L.)

Abstract

RNA molecules function as messengers or noncoding adaptor molecules, structural components, and regulators of genome organization and gene expression. Their roles and regulation are mediated by other molecules they interact with, especially RNA binding proteins (RBPs). Here we report RNA proximity labeling (RPL), an RNA-centric method based on fusion of an endonuclease-deficient Type VI CRISPR-Cas protein (dCas13b) and engineered ascorbate peroxidase (APEX2) to discover *in vivo* target RNA proximal proteins (RPPs) through proximity-based biotinylation. *U1* RPPs enriched by proximity-based biotinylation included both *U1* snRNA canonical and noncanonical functions-related proteins. In addition, profiling of poly(A) tail proximal proteins uncovered expected categories of RBPs for poly(A) tails and also provided novel evidence for poly(A)$^+$ RNA 5'-3' proximity and expanded subcellular localizations. Our results suggest that RPL is a rapid approach for identifying both interacting and neighboring proteins associated with target RNA molecules in their native cellular contexts.

Keywords

Type VI CRISPR-Cas (Cas13), Engineered soybean ascorbate peroxidase APEX2, Proximity-dependent biotinylation, RNA proximity labeling (RPL), RNA proximal proteins (RPPs), RNA-centric method, RNA-protein interactions, poly(A) tail, RNA binding proteins (RBPs), *U1* snRNA interactors.

35 **Introduction**

36 RNA molecules include both messengers encoding proteins (mRNAs) and noncoding
37 RNAs (ncRNAs) such as adaptor tRNAs and regulatory long noncoding RNAs (lncRNAs).
38 Around 2% of the human genome encodes mRNAs (***International Human Genome***
39 ***Sequencing Consortium, 2001; Venter et al., 2001***), while the majority is pervasively
40 transcribed into ncRNAs (***Berretta and Morillon, 2009; Djebali et al., 2012***), including
41 lncRNAs that are widely considered as a large family of potential regulators (***Batista and***
42 ***Chang, 2013; Iyer et al., 2015; Yang et al., 2014***). However, only a small number of
43 lncRNAs have been functionally and mechanistically studied and most remain
44 uncharacterized (***Kopp and Mendell, 2018***).

45 The functions and regulation of RNA transcripts are mediated by other molecules they
46 associate with, particularly RNA binding proteins (RBPs) that govern many critical RNA
47 activities (***Dreyfuss et al., 2002; Glisovic et al., 2008; Hentze et al., 2018; Lunde et al.,***
48 ***2007***). Discovery of the interacting proteins for a given transcript plays pivotal role in
49 unveiling its function and underlying mechanism. Currently, mechanistic study of lncRNAs
50 is impeded by the shortage of RNA-centric tools and the limitations of existing methods
51 (***Ci Chu et al., 2015; Ramanathan et al., 2019***). Antisense probe-based ChIRP (***C. Chu***
52 ***et al., 2015***) or RAP (***McHugh et al., 2015***) requires crosslinking *via* chemicals or UV
53 light. However, chemicals such as formaldehyde also crosslink protein-protein
54 interactions, which may lead to false-positive associations (***Panhale et al., 2019***). Since
55 UV-crosslinking has very low efficiency, antisense probe-based purification methods
56 usually require a large number of cells (~100-800 million) (***Lin et al., 2019; McHugh et***
57 ***al., 2015***), which may not be feasible for slow-growing model systems such as primary

58 cell cultures. Moreover, UV-crosslinking can induce RNA alterations like modifications
59 (***Wurtmann and Wolin, 2009***) that could change binding affinity of RNA to certain RBPs
60 (***Bernard et al., 2012***) and impair downstream protein analysis (***Urdaneta and***
61 ***Beckmann, 2019***). An alternative approach, tagging of endogenous RNA requires
62 genetic manipulation and may interfere with endogenous RNA functions (***Laprade et al.,***
63 ***2020***). Therefore, methods to discover endogenous RNA interacting proteins are needed.
64 In this study, we developed RPL (RNA proximity labelling) method to identify *in vivo*
65 target RNA proximal proteins (RPPs) without crosslinking or genetic manipulation. *U1*
66 RPPs recalled *U1* functional relevant proteins, while poly(A) tail RPPs recalled expected
67 categories of RBPs for poly(A) tails providing additional evidence for poly(A)$^+$ RNA 5'-3'
68 proximity and expanded subcellular localizations.
69

Results

Design and development of RPL, an RNA-centric method for screening RPPs

Inspired by the applications of RNA-targeting Type VI CRISPR-Cas systems (***Abudayyeh et al., 2017; Cox et al., 2017; Konermann et al., 2018; Yan et al., 2018***) and proximity labeling using engineered soybean ascorbate peroxidase (***Lam et al., 2015; Rhee et al., 2013***) and biotin ligase (***Branon et al., 2018; Kim et al., 2016; Roux et al., 2012***), we designed RPL, an RNA-centric approach based on a fusion protein of endonuclease-deficient Cas13 (dCas13) and proximity labeling enzyme APEX2 (***Figure 1A***). The fusion protein is directed to target RNA by a sequence-specific guide RNA (gRNA). In the presence of hydrogen peroxide (H_2O_2), APEX2 in the fusion protein oxidizes substrate biotin-phenol (BP) to short-lived biotin-phenoxyl radicals, which covalently react with electron-rich amino acids (like tyrosine) on RPPs within a small radius (***Rhee et al., 2013***) of the fusion protein (***Figure 1A***). The biotinylated RPPs, which may include target RNA direct binding proteins, indirect binding proteins, and proximal proteins just present within biotinylating radius, can be readily enriched using streptavidin beads and profiled by liquid chromatography-tandem mass spectrometry (LC-MS/MS) (***Figure 1A***).

To construct the fusion protein, Cas13b was used for its high efficacy in RNA knockdown with minimal off-target effect (***Cox et al., 2017***) and high specificity in RNA labeling (***Yang et al., 2019***). For proximity labeling enzyme, we chose APEX2 for its fast kinetics and high activity (***Lam et al., 2015***). Catalytically dead Cas13b from *Prevotella sp. P5-125* (dPspCas13b) (***Cox et al., 2017***) was fused to APEX2 with FLAG and HA tags (***Figure 1B***). The expression of the fusion protein dCas13b-APEX2 (from hereon in called the RPL protein) was confirmed by western blot using an anti-FLAG or anti-HA

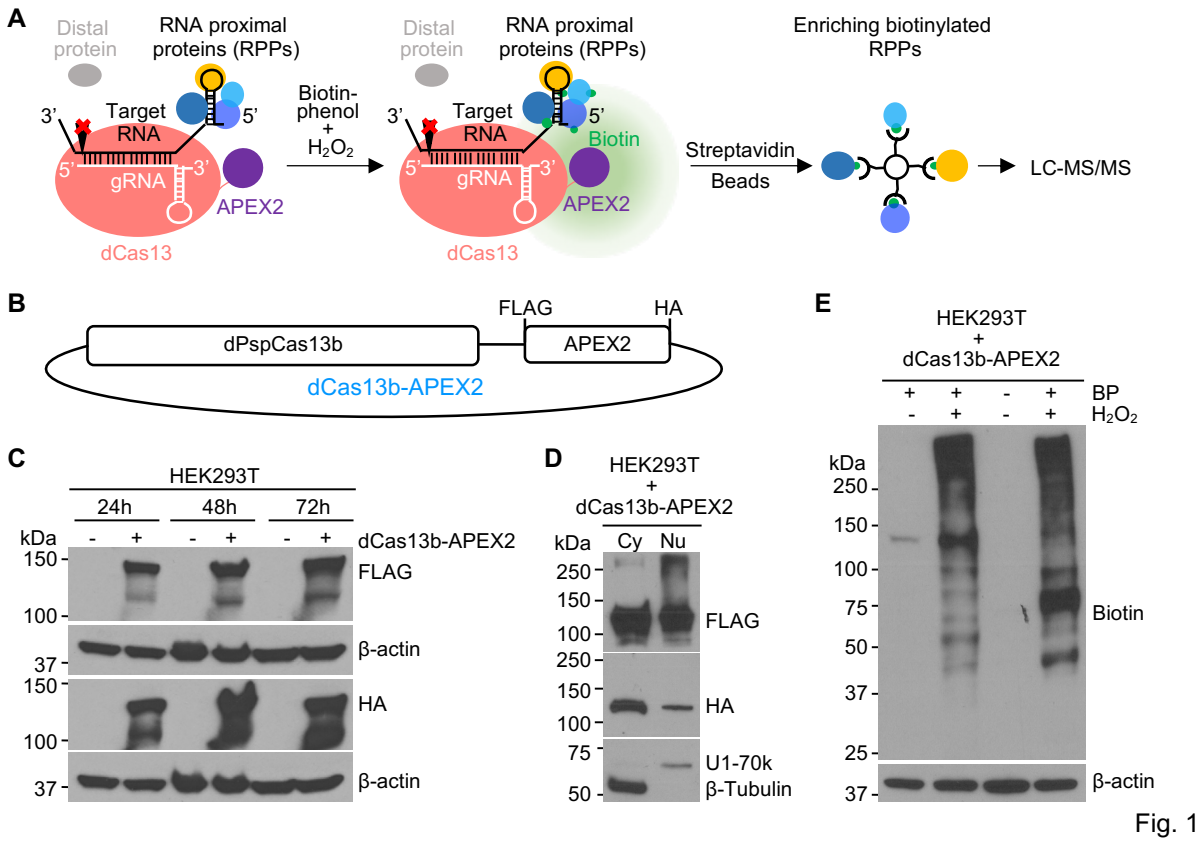

Fig. 1

Figure 1. Designing and developing the RPL method. (**A**). Schematic illustration of RPL workflow. A sequence-specific gRNA directs dCas13-APEX2 to target RNA and APEX2 in the fusion protein biotinylates target RNA proximal proteins (RPPs) *in vivo* in the presence of biotin-phenol and H_2O_2. Biotinylated RPPs are then enriched using streptavidin beads and analyzed by liquid chromatography-tandem mass spectrometry (LC-MS/MS). (**B**). Diagram of the fusion protein dPspCas13b-FLAG-APEX2-HA (dCas13b-APEX2, or the RPL protein) expression construct. (**C**). Expression validation of the RPL protein by western blot. HEK293T cells transfected with or without the RPL plasmid were harvested 24h-72h post transfection and whole cell lysates were blotted with an anti-FLAG or anti-HA antibody. (**D**). The RPL protein is expressed in both cytoplasm and nucleus. HEK293T cells transfected with the RPL plasmid for 24h were fractionated into cytoplasmic (Cy) and nuclear (Nu) fractions. Fractionation efficiency was evaluated by blotting cytoplasmic protein β-Tubulin and nuclear protein U1-70k. (**E**). Validation of enzymatic activity of APEX2 in the RPL protein. HEK293T cells transfected with the RPL plasmid were treated with different combinations of biotin-phenol (BP) and H_2O_2. Whole cell lysates were blotted with anti-biotin antibody. β-actin in (**C**) and (**E**) was used as loading control.

108 antibody (***Figure 1C***). The subcellular localization of the RPL protein was examined when
109 ectopically expressed in HEK293T cells. Efficient separation between cytoplasmic and
110 nuclear fractions was confirmed by blotting for cytoplasmic marker β-Tubulin and nuclear
111 marker U1-70k. The RPL protein was detected in both cytoplasm and nucleus (***Figure***
112 ***1D***). To test if peroxidase activity of APEX2 is maintained in the RPL protein, HEK293T
113 cells were treated with different combinations of BP and H_2O_2 24h post transfection of the
114 RPL plasmid. The detection of biotinylated proteins requires both BP and H_2O_2, indicating
115 that APEX2 in the RPL protein retains peroxidase activity (***Figure 1E***). The results also
116 suggest that endogenous biotinylated proteins are rare in HEK293T cells and low level of
117 endogenous H_2O_2 (***Belousov et al., 2006; Huang and Sikes, 2014; Lyublinskaya and***
118 ***Antunes, 2019***) could not trigger efficient biotinylation. These data suggest that the RPL
119 protein has peroxidase activity and can be applied to target both cytoplasmic and nuclear
120 transcripts.
121

122 **Design and validation of gRNAs targeting *U1* snRNA**

123 To test the approach, we asked whether *U1* snRNA proximal proteins (*U1* RPPs)
124 identified with the RPL protein include any known *U1* RBPs. The *U1* snRNA was selected
125 for three reasons: (1) its high abundance (***Gesteland, 1993***), (2) its structures in human
126 *U1* small nuclear ribonucleoprotein (snRNP) and in spliceosome have been solved
127 (***Charenton et al., 2019; Pomeranz Krummel et al., 2009; Weber et al., 2010***), and (3)
128 its interacting proteins in *U1* snRNP (***Stark et al., 2001***) and in spliceosome (***Zhou et al.,***
129 ***2002***) have been well documented.

130 Since Cas13b targets single-stranded RNA (**Cox et al., 2017; Smargon et al., 2017**),
131 three gRNAs (*U1*-1, *U1*-2, and *U1*-3) targeting *U1* single-stranded regions were designed
132 based on its structure in pre-B complex (**Charenton et al., 2019**) (**Figure 2A**). We first
133 tested if *U1* gRNAs direct wild-type PspCas13b to *U1* and cleave it by measuring *U1*
134 expression in HEK293T cells cotransfected with wild-type PspCas13b plasmid and
135 plasmid expressing *U1* gRNA or nontargeting control (NTC) gRNA at a 1:1 molar ratio.
136 The expression of *U1* was significantly lower in *U1* gRNA-transfected cells compared with
137 NTC gRNA-transfected cells (**Figure 2B**). The expression of a group of nontargets with
138 a wide range of abundance was not affected (**Figure 2B**), except *U2*, which may be
139 caused by Cas13b collateral activity (**Gootenberg et al., 2018**) since *U1* and *U2* are in
140 close contact during spliceosome assembly. The result indicated that *U1* gRNAs can
141 specifically direct PspCas13b to *U1*. We then tested if *U1* gRNAs deliver the RPL protein
142 to *U1* using RNA immunoprecipitation (RIP) experiment. Since the U6 promoter is slightly
143 stronger than CMV promoter in HEK293T cells (**Lebbink et al., 2011**), a 1:2 molar ratio
144 between the RPL plasmid (CMV promoter) and gRNA expressing plasmid (U6 promoter)
145 was used to avoid nonspecific targeting due to excess RPL protein. The RPL protein was
146 efficiently retrieved by anti-HA but not isotype control IgG (**Figure 2C**). Analysis of RNA
147 extracted from RIP experiment showed that anti-HA pulled down 5 times more RNA than
148 control (**Figure 2D**), certifying the RPL protein RNA binding activity. Although there is no
149 significant difference in the amount of RNA pulled down by the RPL protein with NTC or
150 *U1* gRNAs (**Figure 2D**), *U1* gRNAs significantly enriched *U1* for ~2-3-fold compared with
151 NTC gRNA (**Figure 2E**). The fact that much more abundant *18S* was not enriched (**Figure
152 2E**) suggested that *U1* gRNAs are able to specifically direct the RPL protein to *U1*.

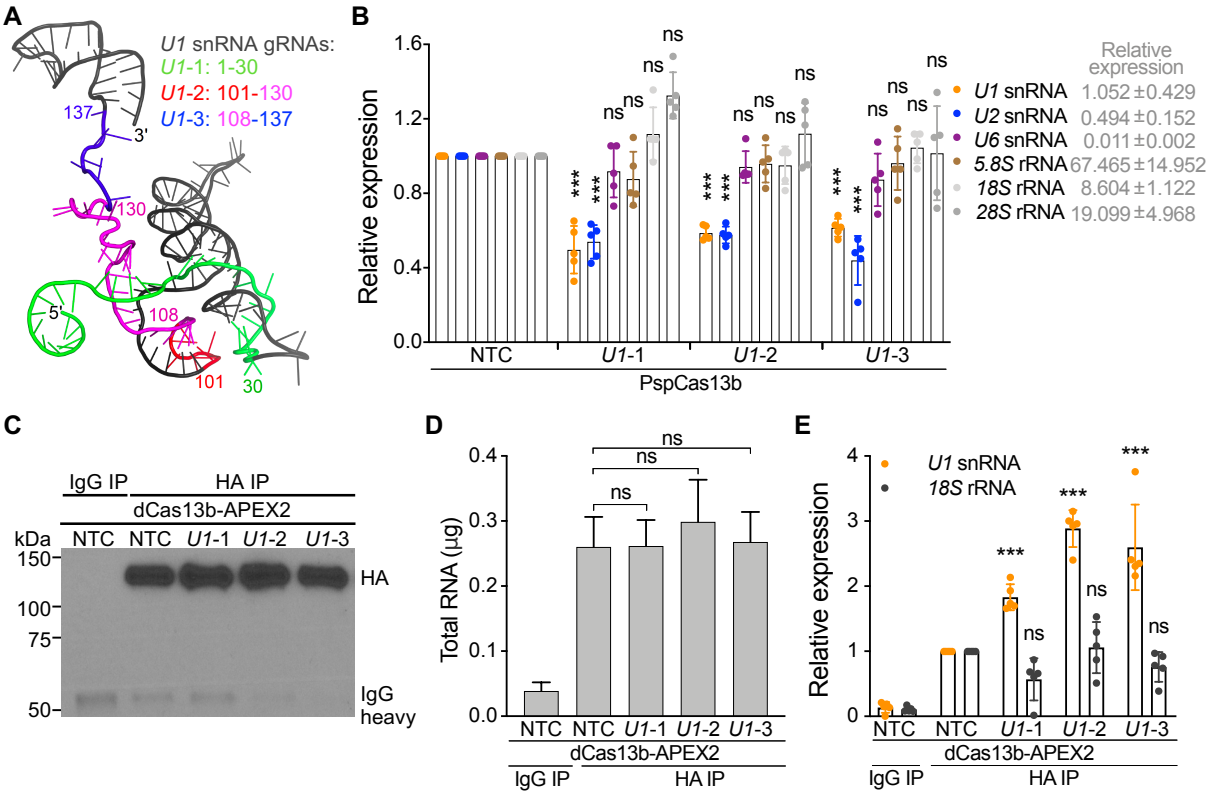

Fig. 2

Figure 2. Designing and validating gRNAs targeting *U1* snRNA. (**A**). Based on *U1* structure, three gRNAs with spacers targeting *U1* nucleotides (nt) 1-30 (*U1*-1), 101-130 (*U1*-2), and 108-137 (*U1*-3) were designed. Cartoon representation of *U1* (PDB ID: 6QX9, pre-B complex) is colored in black, 1-30 in green, 101-107 in red, 108-130 in magenta, and 131-137 in blue. (**B**). The expression of *U1* snRNA was significantly downregulated in *U1* gRNA-transfected cells. HEK293T cells were cotransfected with plasmid expressing wild-type PspCas13b and plasmid expressing *U1* or NTC gRNA (1:1 molar ratio). The expression of *U1* or a group of nontargets was quantified by RT-qPCR and normalized to *GAPDH*. (**C**). Confirmation of pulldown of the RPL protein by RIP using western blot. HEK293T cells were cotransfected with the RPL plasmid and plasmid expressing *U1* or NTC gRNA (1:2 molar ratio). Anti-HA antibody or isotype control IgG were used to immunoprecipitate the RPL protein. Clean-Blot IP detection reagent was used for blotting. (**D**). The amount of total RNA extracted from RIP experiment. (**E**). *U1* gRNAs specifically directed the RPL protein to *U1*. The expression of *U1* snRNA and nontarget *18S* rRNA was quantified by RT-qPCR and normalized to *GAPDH*. Data shown in (**B**), (**D**), and (**E**) are mean ± SD from 5 independent experiments. ***p<0.001, ns, not significant. Student's *t* test.

168 **RPL-MS identified both *U1* canonical and noncanonical roles-related proteins**

169 We next enriched *U1* RPPs using RPL with the same 1:2 molar ratio to avoid excess RPL
170 protein that can cause nonspecific targeting and proximity labeling. *U1* has compact
171 structure in pre-B complex (***Charenton et al., 2019***) (***Figure 2A***) and its size (less than
172 ~10 nm in diameter) is much smaller than the biotinylating range of APEX2 (likely ~20-40
173 nm or larger in diameter) (***Fazal et al., 2019; Padrón et al., 2019; Rhee et al., 2013***), so
174 we considered experiments using our three *U1* gRNAs as replicates. We analyzed
175 streptavidin-enriched biotinylated proteins by LC-MS/MS (RPL-MS). Using label-free
176 intensity-based absolute quantification (iBAQ) values to measure enrichment in *U1* gRNA
177 relative to protein amounts in the NTC gRNA sample, RPL-MS identified 226 *U1* RPPs (p
178 < 0.05 and $\log_2$ fold change [FC] > 2, false discovery rate [FDR] < 0.25, Benjamini-
179 Hochberg method), including known *U1* direct RBPs (e.g. SNRNP70, also known as U1-
180 70k) (***Stark et al., 2001***) and RBPs that likely interact with *U1* indirectly due to their
181 function in the spliceosome (e.g. SNRPA1 and SNRPB2) (***Zhou et al., 2002***) (***Figure 3A,***
182 ***Table S1***). We verified the enrichment of U1-70k using western blot and found that it was
183 enriched ~2-fold by all three *U1* gRNAs (***Figure 3B***), consistent with RPL-MS results
184 (***Figure 3A***). Analysis of KEGG pathways enriched in the group of *U1* RPPs using
185 STRING (***Szklarczyk et al., 2019***) showed that 'Spliceosome' is the most significantly
186 enriched pathway (FDR < 10^{-8}) (***Figure 3C***). Indeed, *U1* RPPs included 99 splicing and
187 related factors (***Cvitkovic and Jurica, 2013***), 56 proteins previously found by *U1* ChIRP-
188 MS (***C. Chu et al., 2015***), and 58 proteins revealed by XLIP-MS using anti-U1A and/or
189 anti-U1-70k antibody (***So et al., 2019***) (***Figure 3D***). In addition, the binding between *U1*
190 and four *U1* RPPs was further supported by corresponding CLIP-Seq data as shown in

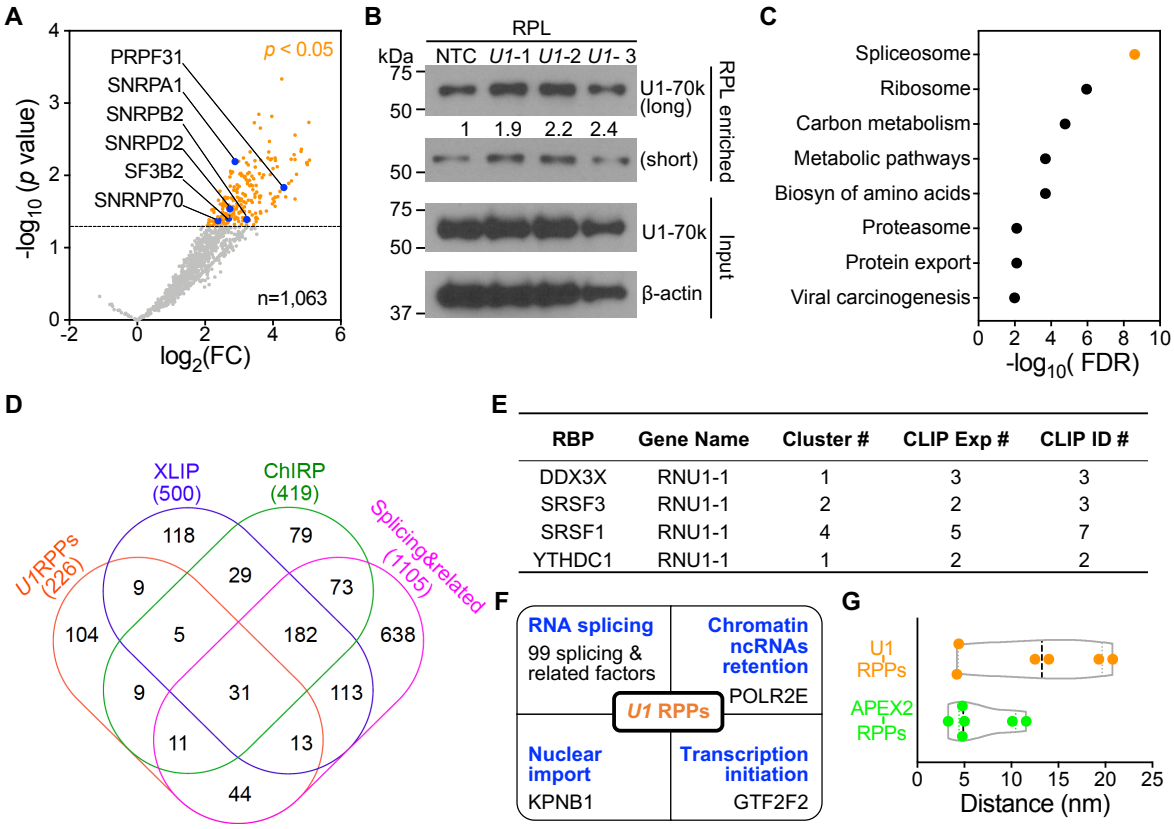

RBP	Gene Name	Cluster #	CLIP Exp #	CLIP ID #
DDX3X	RNU1-1	1	3	3
SRSF3	RNU1-1	2	2	3
SRSF1	RNU1-1	4	5	7
YTHDC1	RNU1-1	1	2	2

Fig. 3

Figure 3. *U1* RPPs identified by RPL-MS. (**A**). *U1* RPPs revealed by RPL-MS include known *U1* RBPs. Volcano plot shows *U1*/NTC iBAQ ratio (fold change, FC) of protein quantification in *U1* gRNA cells compared with NTC gRNA cells. RPL-MS enriched 226 *U1* RPPs (orange dots) that were statistically significant ($p < 0.05$ and $\log_2$ FC > 2, FDR < 0.25, Benjamini-Hochberg method). Each dot represents the average value from experiments using three *U1* gRNAs. Blue dots represent proteins from pre-B spliceosome complex. (**B**). *U1* direct RBP U1-70k was enriched by RPL. HEK293T cells transfected with the RPL plasmid and plasmid expressing *U1* gRNA or NTC gRNA were treated with BP and H_2O_2. Whole cell lysates (Input) or streptavidin-enriched biotinylated proteins (RPL enriched) were blotted. Numbers represent relative amount of U1-70k under the corresponding conditions from RPL enriched normalized to input. (**C**). KEGG pathways significantly enriched by 226 *U1* RPPs using STRING. (**D**). Comparison of *U1* RPPs, *U1* interactors identified by ChIRP-MS, *U1* interactors identified by XLIP-MS using anti-U1A and/or anti-U1-70k antibody, and splicing & related proteins. Numbers listed below are total number of proteins from each group. (**E**). List of 4 *U1* RPPs with CLIP-Seq data supporting their association of *U1* found in

205 ENCORI. (**F**). Summary of *U1* RPPs related to *U1* functions. (**G**). Inferred distances between *U1* or APEX2
206 in the RPL protein and those 6 *U1* RPPs present in pre-B complex shown in (**A**).
207
208 ENCORI (***Li et al., 2014***), including DDX3X that is not known to interact with *U1* in human
209 (***Deckert et al., 2006; Tarn and Chang, 2009***) (***Figure 3E***). These results together
210 validated that RPL can efficiently identify most known RBPs for *U1*.
211 *U1* RPPs also included previously reported *U1* interactor RNA polymerase II (***Spiluttini***
212 ***et al., 2010; Yu and Reed, 2015***) (***Figure 3F***), which is required for a noncanonical role
213 of *U1* in chromatin retention of ncRNAs (***Yin et al., 2020***). Moreover, *U1* RPL retrieved
214 proteins involved in chromatin remodeling, DNA modification, histone modification, and
215 transcription (***Table S1***), which could be regulated by chromatin-associated ncRNAs
216 (***Huang et al., 2020; Li and Fu, 2019***). The presence of GTF2F2 among the *U1* RPPs
217 may relate to a role for *U1* in regulation of transcription initiation (***Damgaard et al., 2008;***
218 ***Kwek et al., 2002***) (***Figure 3F***). Interestingly, RPL-MS revealed nuclear import receptor
219 importin-β1 (KPNB1) (***Figure 3F***), which is required for *U1* nuclear import (***Palacios,***
220 ***1997***). Six RBPs in pre-B complex (***Charenton et al., 2019***) were identified as *U1* RPPs
221 (***Figure 3A***). Their distances to *U1* snRNA in pre-B complex may provide insight to the
222 biotinylating range of the RPL protein. The inferred distances between APEX2 in the RPL
223 protein and those RBPs are all smaller than 12 nm and the average is 6.6 nm (***Figure***
224 ***3G***), suggesting that APEX2 may biotinylate proteins within 12 nm. The inferred distances
225 between *U1* and associated RBPs range from 4.2 nm to 20.8 nm with an average of 12.5
226 nm (***Figure 3G***), suggesting that RPL can biotinylate proximal proteins within ~20 nm of
227 target RNA. These data indicated that RPL enables efficient identification of validated
228 RBPs associated with both canonical and noncanonical functions of *U1*.

229

230 **RPL-MS recalled expected categories of proteins for poly(A) tails**

231 To further test the generality of RPL method, we applied it to poly(A) tails, which are
232 adenosines added to the 3' ends of the majority of eukaryotic mRNAs and many lncRNAs
233 in the absence of template (***Derrien et al., 2012; Guttman et al., 2009; Tian, 2005; Yang***
234 ***et al., 2011***). Poly(A) tails play critical role in mRNA translation and stability (***Dreyfus and***
235 ***Régnier, 2002***) and their removal triggers mRNA decapping and decay (***Muhlrad et al.,***
236 ***1994; Norbury, 2013; Yamashita et al., 2005***). Although the 5' and 3' ends of pre-
237 translational mRNAs (***Metkar et al., 2018***) and deadenylating mRNAs (***Chen and Shyu,***
238 ***2011***) are distant (***Figure 4A, 5'-3' distance***), the physical distances between the two
239 ends of diverse RNAs are incredibly close regardless of their length, type, species, or
240 complexity (***Lai et al., 2018; Leija-Martínez et al., 2014***) (***Figure 4A, 5'-3' proximity***).
241 As oligomers of 30 nt poly(U) are not found at the 3' of RNA (***Chang et al., 2014; Lim et***
242 ***al., 2018***) and rarely occur in the human transcriptome, poly(U)-targeting gRNA, or poly(U)
243 gRNA, was used as negative control. The RPL plasmid was cotransfected with plasmid
244 expressing poly(A) or poly(U) gRNA into HEK293T cells at a 1:2 molar ratio and then RPL
245 was performed. Using label-free iBAQ values to measure enrichment in poly(A) gRNA
246 relative to protein amounts in the poly(U) gRNA sample, RPL-MS enriched 786 proteins
247 as poly(A) tail RPPs (Benjamini-Hochberg-adjusted $p < 0.05$ and $\log_2 FC > 2$) (***Figure 4B,***
248 ***Table S2***). Poly(A) tail RPPs included seven poly(A) binding proteins, fifteen 3'UTR
249 binding proteins, ten 5'UTR binding proteins, and one cap binding protein (***Figure 4B,***
250 ***Table S3***), all of which are known to associate with poly(A) tails. Retrieval of proteins from
251 both 5' and 3' ends by RPL within a small radius provided additional evidence for poly(A)$^+$

252 RNA 5'-3' proximity.

253 Among poly(A) tail RPPs, at least 48% were RBPs interacting with poly(A)$^+$ RNA (***Baltz***
254 ***et al., 2012; Castello et al., 2012; Kwon et al., 2013; Milek et al., 2017***) (***Figure 4C***). In
255 theory, poly(A) gRNA can direct the RPL protein to any transcripts with 30 nt-poly(A) tail
256 or longer (***Figure 4A***), including transcripts undergoing polyadenylation, readenylation,
257 deadenylation, or translation. We then interrogated poly(A) tail RPPs for other expected
258 classes of proteins, including factors involved in polyadenylation (***Shi and Manley, 2015***),
259 readenylation or deadenylation (***Yan, 2014***), and translation (***Dreyfus and Régnier,***
260 ***2002***). Indeed, RPL-MS enriched five cleavage and polyadenylation factors for poly(A)$^+$
261 RNA (***Figure 4D***) but no such factors unique for poly(A)$^-$ RNA (e.g. SLBP and ZNF473)
262 (***Gilmartin, 2005***) (***Table S3***). Moreover, poly(A) tail RPPs included three exosome
263 proteins (***Chlebowski et al., 2013***), two deadenylase complex proteins (***Collart, 2016***),
264 as well as decapping factor EDC3 (***Mugridge et al., 2018***) (***Figure 4D, Table S3***).
265 Importantly, twenty translation initiation factors, fifteen translation elongation factors,
266 seventy ribosomal subunits, and eighteen tRNA ligases were identified by RPL-MS
267 (***Figure 4D, Table S3***), putatively supporting a model that poly(A) tail recruits translation
268 initiation factors to initiate translation at the 5' end like their viral counterparts (***Simon and***
269 ***Miller, 2013; Truniger et al., 2017***). Moreover, RPL-MS revealed twelve proteins
270 involved in degradation of AU-rich element-containing mRNAs and 66 nonsense-
271 mediated decay proteins (including 58 ribosomal subunits) (***Chang et al., 2007; Laroia***
272 ***et al., 2002, 1999***) (***Table S3***), further suggesting that RPL enables efficient discovery of
273 most relevant and validated RBPs proximal to poly(A) tails.

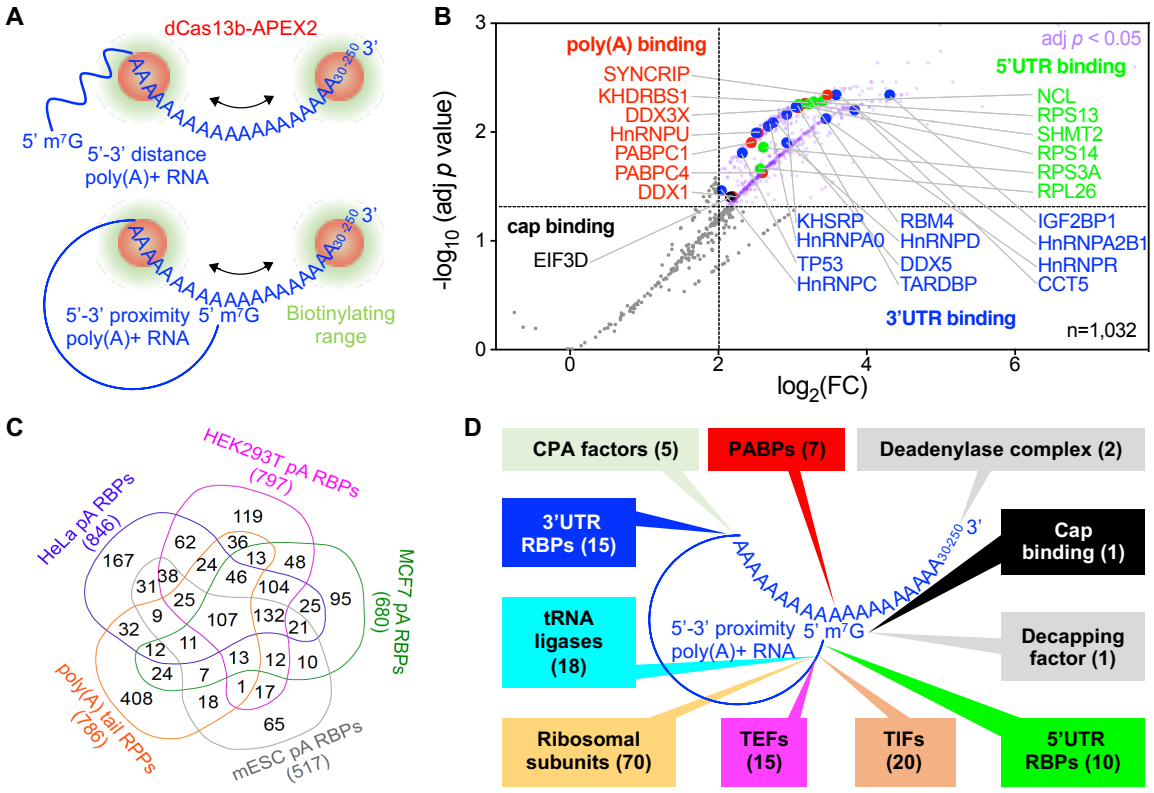

Fig. 4

Figure 4. RPL-MS revealed poly(A) tail RPPs in HEK293T cells. (**A**). Application of RPL to poly(A) tails. In the presence of gRNA, the RPL protein (dCas13b-APEX2) is directed to poly(A) tails ranging from 30 nt up to ~250 nt. In 5'-3' distance model, RPL will detect PABPs and 3'UTR binding proteins that bind proximal to poly(A) tail within the biotinylating range. In 5'-3' proximity model, RPL will also identify cap-binding proteins and 5'UTR binding proteins that bind proximal to the cap and lie within the biotinylating range. (**B**). RPL-MS identified poly(A) tail RPPs. Volcano plot shows RPL-labeled proteins in HEK293T cells. For each protein, the poly(A)/poly(U) iBAQ ratio reflects the enrichment of identified protein in poly(A) gRNA cells compared with poly(U) gRNA transfected cells. RPL-MS identified 786 proteins (light purple dots) as significantly enriched (Benjamini-Hochberg-adjusted $p < 0.05$ and $\log_2 FC > 2$). Each data point represents the average value from biological triplicates. Red dots represent proteins belonging to PABPs, blue dots for 3'UTR binding proteins, green dots for 5'UTR binding proteins, and black dot for cap binding protein. (**C**). Venn diagram shows the comparison of poly(A) tail RPPs and RBPs associated with poly(A)$^+$ RNA in different cells. Numbers below each group represent the sizes of the protein cohort. (**D**). Summary of expected categories of poly(A) tail RPPs that support 5'-3' proximity and the role of poly(A) tail in mRNA

289 translation. Each category of proteins points to a location/region of poly(A)$^+$ RNA where they most likely
290 associate with when identified by RPL. PABPs, poly(A) binding proteins; CPA, cleavage and
291 polyadenylation; TIFs, translation initiation factors; TEFs, translation elongation factors.
292

293 **Localization analysis of poly(A) tail RPPs unveils expanded subcellular**
294 **localizations for poly(A)$^+$ RNA**

295 Poly(A) tails are important for RNA nuclear export (***Huang and Carmichael, 1996***) *via*
296 the nuclear pore complex (NPC) (***Okamura et al., 2015***). This is further supported by the
297 presence of 90 mRNA processing factors, 20 mRNA nuclear export proteins, and 13 NPC
298 proteins in poly(A) tail RPPs (***Figure 5A***). It is not surprising that tRNAs and pre-miRNAs
299 nuclear export factors were also included (***Table S3***) since their precursors or primary
300 transcripts are also polyadenylated (***Cai, 2004; Kadaba et al., 2006***). Poly(A) tail RPPs
301 contained eight tRNA processing factors and five tRNA nuclear export factors (***Kruse et***
302 ***al., 2000***), as well as three pri-miRNA processing factors and two pre-miRNA export
303 factors (***Bohnsack et al., 2004; Lund et al., 2004; Yi et al., 2003***) (***Table S3***), supporting
304 that their processing is coupled with export (***Kim, 2005; Köhler and Hurt, 2007***). Poly(A)
305 tail RPPs recovered 27 RBPs involved in mRNA transport (including zipcodes binding
306 protein IGF2BP1), 48 microtubule proteins, and 139 plasma membrane proteins that are
307 used by mRNAs to achieve different subcellular localizations (***Holt and Bullock, 2009;***
308 ***Mofatteh and Bullock, 2017***) (***Figure 5A***), possibly suggesting a role for the poly(A) tail
309 in RNA subcellular localization.

310 Since unique localizations of RPPs reflect target RNA proximal localizations, we built
311 a putative subcellular localization map for poly(A)$^+$ RNA by comparing poly(A) tail RPPs
312 with proteins extracted from 22 subcellular compartments (***Figure 5B, Table S3***). The

313 results are generally consistent with previous reports that both mRNAs and ncRNAs have
314 multiple subcellular localizations (***Blower, 2013; Carlevaro-Fita and Johnson, 2019;***
315 ***Fazal et al., 2019; Wilk et al., 2016***) and also support the presence of mRNAs in P-
316 bodies, stress granule, and the exosome (***Chlebowski et al., 2013; Decker and Parker,***
317 ***2012***). Interestingly, RPL-MS also identified marker proteins of the endosome, lysosome,
318 proteasome, and Golgi apparatus, indicative of expanded subcellular localizations for
319 poly(A)$^+$ RNA (***Figure 5B, Table S3***). Discovery of lysosomal and proteasomal proteins
320 in poly(A) tail RPPs is compatible with the existence of RNA degradation pathway
321 'RNautophagy' in the lysosome (***Fujiwara et al., 2013***) and degradation function of
322 proteasomes for AU-rich element-containing mRNAs (***Laroia et al., 2002, 1999***). The
323 identification of endosomal proteins is in accordance with that late endosomes can be
324 used by mRNAs as a platform for translation (***Cioni et al., 2019***). Poly(A) tail RPPs
325 included Golgi marker *cis*-Golgi matrix protein GOLGA2 (***Munro, 2011***) (***Table S3***), which
326 has recently been annotated as an RBP by multiple groups (***Caudron-Herger et al., 2019;***
327 ***Queiroz et al., 2019; Trendel et al., 2019***), suggesting that Golgi may be a novel
328 subcellular location for poly(A)$^+$ RNA. More experimental data are needed to determine
329 which specific transcripts are associated with GOLGA2 in the Golgi apparatus and the
330 biological significance of those interactions.
331

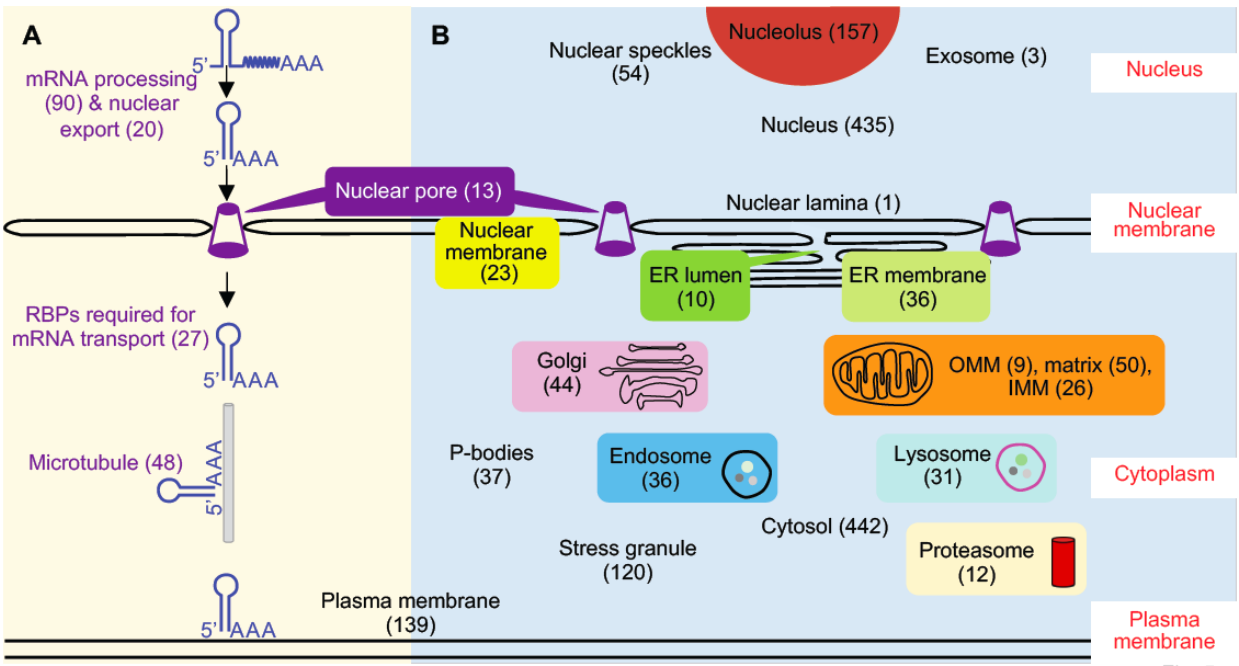

Figure 5. Poly(A) tail RPPs included proteins involved in subcellular localization of RNA. (**A**). RPL-MS revealed proteins involved in RNA processing, nuclear export, transport, and subcellular localization for poly(A) tail RPPs. (**B**). A putative subcellular localization map of poly(A)$^+$ RNA built upon subcellular localization of poly(A) tail RPPs. Poly(A) tail RPPs were compared with proteins extracted from corresponding GO terms. Numbers in brackets represent the size of each category of proteins. A full list of proteins in each category can be found in ***Table S3***.

Discussion

RPL: an RNA-centric approach for RPPs identification in living cells

We present an RNA-centric method, RPL, for discovering RPPs for transcripts of interest and evaluate it in two distinct contexts–first interrogating a specific ncRNA target *U1* and second surveying a heterogenous group of poly(A)$^+$ RNA in living cells. Both *U1* RPPs and poly(A) tail RPPs demonstrated that RPL enables efficient discovery of functional relevant RBPs for target transcripts. The recall of KPNB1 for *U1* nuclear import suggests that RPL allows to detect transient and/or weak interacting proteins (***Branon et al., 2017;***

348 ***Roux et al., 2013***). Compared with alternative methods, RPL needs no crosslinking or
349 sonication, requires far fewer cells (~20-40 million vs ~100-800 million) and involves no
350 genetic manipulation, which may interfere target RNA functions (***Laprade et al., 2020***).
351 The short pulse of labeling potentially permits RPL to be applied to study RNA-protein
352 dynamics. Recently, APEX2 has also been reported to biotinylate proximal nucleic acids
353 (***Fazal et al., 2019; Padrón et al., 2019; Y. Zhou et al., 2019***), suggesting that RPL could
354 be potentially applied to identify RNA and DNA in addition to proteins proximal to the
355 target RNA (together as 'RNA proximitome') within living cells.

356 During the preparation of our manuscript, similar strategies using different fusion
357 proteins of endonuclease-deficient Cas13 protein (dLwaCas13a, dPspCas13b, and
358 dRfxCas13d) and proximity labeling enzyme (APEX2, BioID2, BASU, and PafA) were
359 reported (***Han et al., 2020; Li et al., 2020; Yi et al., 2020; Zhang et al., 2020***).
360 Applications of these methods together with ours to both mRNAs and ncRNAs with wide
361 range of abundance (~10^2-10^6 copies/cell) demonstrate that these methods have broad
362 potential to identify functional relevant RBPs for diverse transcripts.

363 RPPs identified using the dCas13b-APEX2 are expected to include three types of
364 proteins theoretically: proteins that directly bind to target RNA, proteins that associated
365 with target RNA indirectly via protein-protein interactions, and proteins present within the
366 biotinylating range. Biological replicates are expected to help enrich the first two groups
367 of RBPs and reduce the third type as false positive candidates may not be enriched
368 repeatedly. In addition, an optimal molar ratio between the fusion protein and gRNA,
369 which enables efficient proximity-based biotinylation and prevents nonspecific labeling
370 due to excess fusion protein, is crucial for separating signal from noise. A validated set of

371 gRNAs that can specifically direct fusion protein to target RNA with low off-target activity
372 is another key factor. As complementarity between the gRNA spacer and targeted region
373 as well as local RNA accessibility are essential for RNA targeting (***Abudayyeh et al.,***
374 ***2017; Cox et al., 2017; Konermann et al., 2018; Smargon et al., 2017***), general
375 principles for gRNA designing can provide critical help in choosing spacer sequence and
376 length for gRNA aiming at single-stranded region of target RNA (***Bandaru et al., 2020;***
377 ***Wessels et al., 2020***).
378

379 **Limitations and directions for improvement**

380 High concentration of H_2O_2 (1 mM) used in the RPL method may cause oxidative stress
381 and necrosis to the cells (***Clément and Pervaiz, 2001***) and may preclude the application
382 of RPL to systems sensitive to oxidative stress and cell harm. Similar to other fusion
383 proteins, the RPL protein due to its large size (~130kDa) may pose steric hindrance to
384 access target RNA and increase the biotinylating range, which could reduce specificity
385 and limit the application to mapping RNA functional domains (***Quinn et al., 2014***) and
386 RNA-protein interactions at high resolution. Improvement could be achieved using smaller
387 Cas13 proteins by structure-guided truncations (***Zhang et al., 2018***). Alternatively, CIRTS
388 strategy could be applied to assemble a much smaller gRNA-dependent RNA proximity
389 labeling enzyme (***Rauch et al., 2019***).

390 Another limitation is that RPL and similar tools may not identify RBPs for a target RNA
391 as efficiently as antisense probe-based methods, as the RPL protein has to compete with
392 the RBPs bound to the target transcript (***Wessels et al., 2020***). The RPL protein can only
393 access single-stranded regions of target RNA (***Cox et al., 2017; Smargon et al., 2017***)

394 and only proteins with electron-rich amino acids like tyrosine exposed on the surface
395 within the biotinylating range have the opportunity to be labeled (***Rhee et al., 2013***). The
396 same limitation also applies to other proximity labeling enzymes including BioID and its
397 relatives and PafA, which all favor lysine as labeling substrate (***Liu et al., 2018;***
398 ***Samavarchi-Tehrani et al., 2020***).
399
400 **Perspectives**
401 We anticipate that RPL and similar methods will be widely applied to characterize the
402 functions and regulation of diverse categories of RNA in multiple cell types and organisms.
403 Since both Cas13s and proximity labeling are very active research areas, further
404 optimization and refinements of RPL and similar methods are expected. Utilizations of
405 these tools together with protein-centric methods (***Licatalosi et al., 2008; Van Nostrand***
406 ***et al., 2016***), annotation of RNA structure (***Spitale et al., 2015; Sun et al., 2019***) could
407 shed light on the molecular mechanisms of lncRNA functions, RNA-protein interactions,
408 RNA functional domain, and binding specificities for RBPs.
409
410 **Acknowledgements**
411 This work was supported by the Ovarian Cancer Research Alliance (Ann and Sol
412 Schreiber Mentored Investigator Award 458799 to X.L.) and the National Cancer Institute
413 (K99/R00-CA184415 and R01-CA207456 to K.L.), the Cedars-Sinai Samuel Oschin
414 Comprehensive Cancer Institute (Cancer Biology Grant 231433 to K.L.). We thank Drs.
415 Wei Yang and Bo Zhou at the Cedars-Sinai Medical Center Biomarker Discovery Platform

Core for label-free quantitative mass spectrometry analysis. We also thank anonymous reviewers for their insightful comments and suggestions.

Author contributions

X.L conceived the project, designed and performed all experiments, and analyzed the data. R.I.C. and M.A.S.F. analyzed the data. K.L. supervised the project. X.L. and K.L. wrote the manuscript with input from all authors.

Competing interests

The authors declare no competing interests.

426 ## Materials and methods

427 ## Key Resources Table

Reagent or Resource	Source	Identifier
Antibodies		
U1-70k	EMD Millipore	Cat.# 05-1588, RRID: AB_11210916
β-tubulin	Sigma Aldrich	Cat.# T8328, RRID: AB_1844090
HA	Santa Cruz	Cat.# sc-7392, RRID: AB_627809
FLAG	Santa Cruz	Cat.# sc-166384, RRID: AB_2017592
Biotin	Santa Cruz	Cat.# sc-57636, RRID: AB_628778
β-actin	Santa Cruz	Cat.# sc-47778, RRID: AB_626632
IgG	Thermo Fisher Scientific	Cat.# 10500C, RRID: AB_2532981
Chemicals		
biotin-phenol	Iris Biotech	Cat.# LS-3500.1000, RRID: N/A
hydrogen peroxide (H_2O_2)	Sigma Aldrich	Cat.# H1009, RRID: N/A
sodium azide	Sigma Aldrich	Cat.# S2002-5G, RRID: N/A
sodium ascorbate	Sigma Aldrich	Cat.# PHR1279-1G, RRID: N/A
Trolox	Sigma Aldrich	Cat.# 238813-1G, RRID: N/A
Dynabeads Protein A	Thermo Fisher Scientific	Cat.#: 10001D, RRID: N/A
Streptavidin magnetic beads	Thermo Fisher Scientific	Cat.# 88817, RRID: N/A
Plasmids		
pC0046-EF1a-PspCas13b-NES-HIV	Addgene	RRID: Addgene_103862
pC0053-CMV-dPspCas13b-GS-ADAR2DD (E488Q)-delta-984-1090	Addgene	RRID: Addgene_103869
pCMV-dPspCas13b-FLAG-APEX2-HA	This study	N/A
pcDNA3-APEX2-NES	Addgene	RRID: Addgene_49386
PspCas13b NTC gRNA	Addgene	RRID: Addgene_103854
PspCas13b U1-1 gRNA	This study	N/A
PspCas13b U1-2 gRNA	This study	N/A
PspCas13b U1-3 gRNA	This study	N/A
PspCas13b poly(A) gRNA	This study	N/A
PspCas13b poly(U) gRNA	This study	N/A
Experimental Models: Cell lines		
Human HEK293T cells	ATCC	Cat.# CRL-3216, RRID: CVCL_0063
Software and Algorithms		
PyMOL	PyMOL	RRID: SCR_000305
Metascape	Metascape	RRID: SCR_016620
STRING	STRING	RRID: SCR_005223
Limma	Limma	RRID: SCR_010943

428

429 **Plasmids and cloning.** pC0046-EF1a-PspCas13b-NES-HIV was a gift from Dr. Feng Zhang (Addgene
430 plasmid # 103862). pCMV-dPspCas13b-FLAG-APEX2-HA (RPL plasmid) was constructed by replacing
431 ADAR2DD-delta-984-1090 in pC0053-CMV-dPspCas13b-GS-ADAR2DD (E488Q)-delta-984-1090 (a gift
432 from Dr. Feng Zhang, Addgene plasmid # 103869) with FLAG-APEX2-HA subcloned from pcDNA3-

433 APEX2-NES (a gift from Dr. Alice Ting, Addgene plasmid # 49386) using the following primers:
434 dPspCas13b-For: 5'TACCCATACGATGTTCCAGATTACGCTTAAGCGGCCGCTCGAGTC3',
435 dPspCas13b-Rev: 5'GTCGTCATCCTTGTAGTCGGATCCCAGTGTCAGTCTTTCAAG3',
436 FLAG-APEX2-HA-For: 5'GACTACAAGGATGACGACG3',
437 FLAG-APEX2-HA-Rev: 5'TGGAACATCGTATGGGTACTGCAGGGCATCAGCAAAC3'.
438 PCR was performed using Q5 High-Fidelity DNA Polymerase (New England Biolabs, Cat.# M0491L). PCR
439 fragments were assembled using NEBuilder HiFi DNA Assembly Master Mix (New England Biolabs, Cat.#
440 E2621S) according to manufacturer's instructions. The following spacer sequences were used to express
441 gRNAs using pC0043-PspCas13b crRNA backbone (a gift from Dr. Feng Zhang, Addgene plasmid #
442 103854):
443 NTC: ATGTCTTCCTGGGACGAAGACAA
444 *U1*-1_{1-30} : ATCATGGTATCTCCCCTGCCAGGTAAGTAT,
445 *U1*-$2_{101-130}$: CAAATTATGCAGTCGAGTTTCCCACATTTG,
446 *U1*-$3_{108-137}$: ACTACCACAAATTATGCAGTCGAGTTTCCC,
447 Poly(A): TTTTTTTTTTTTTTTTTTTTTTTTTTTTTT,
448 Poly(U) : AAAAAAAAAAAAAAAAAAAAAAAAAAAAAA.
449 The sequences of all constructs have been confirmed using Sanger sequencing.
450
451 **Transfection and *in vivo* proximity dependent biotinylation.** For validation of *U1* gRNAs in directing the
452 RPL protein to target *U1*, HEK293T cells were seeded into 12-well plates and were transfected with 1.5 μg
453 the RPL plasmid and 0.5 μg Cas13b gRNAs (NTC, *U1*-1, *U1*-2, *U1*-3) while ~80% confluency using
454 Lipofectamine 3000 (Thermo Fisher Scientific, Cat.# L3000015). For RIP experiments, HEK293T cells were
455 seeded into 6-well plates and were transfected with 2.5 μg the RPL plasmid and 1.5 μg Cas13b gRNAs
456 while ~80% confluency using Lipofectamine 3000. For proximity-dependent biotinylation, HEK293T cells
457 were seeded into 150 mm plate and were transfected with 25 μg the RPL plasmid and 15 μg Cas13b gRNAs
458 (NTC, *U1*-1, *U1*-2, *U1*-3, poly[A], poly[U]) while ~80% confluency using Lipofectamine 3000. HEK293T cells
459 were incubated with 25 mL of DMEM media containing 25 μL of 500 mM biotin-phenol (Iris Biotech, Cat.#
460 LS-3500.1000) in DMSO for 30 min at 37 °C 24h post transfection. Cells were then treated with 1 mM

461 hydrogen peroxide (H_2O_2) (Sigma Aldrich, Cat.# H1009) for 1 min on a horizontal shaker at room
462 temperature. The labeling solution was aspirated and cells were washed twice with 25 mL of quencher
463 solution (10 mM sodium azide [Sigma Aldrich, Cat.# S2002-5G], 10 mM sodium ascorbate [Sigma Aldrich,
464 Cat.# PHR1279-1G], and 5 mM Trolox [Sigma Aldrich, Cat.# 238813-1G] in DPBS (Thermo Fisher Scientific,
465 Cat.# 14040182). Cells were then washed three times with 15 mL of DPBS and were pelleted by
466 centrifugation at 1,500 g for 5 min at 4 °C. Cell pellets were snap frozen and stored at −80 °C.
467
468 **Streptavidin enrichment of biotinylated proteins.** Cell pellets from two 150 mm plates of transfected
469 HEK293T cells were lysed in 2 mL cell lysis buffer (10 mM HEPES, pH7.5 by KOH, 150 mM NaCl, 0.1%
470 NP-40, 5 mM EGTA, 5 mM Trolox, 10 mM Sodium ascorbate acid, 10 mM Sodium azide, 1 mM PMSF).
471 Streptavidin magnetic beads (Thermo Fisher Scientific, Cat.# 88817) were washed twice with cell lysis
472 buffer and 3.5 mg of each whole cell lysate sample were incubated with 100 µL magnetic bead slurry with
473 rotation for 2 h at room temperature. After enrichment, the flowthrough was removed and beads were
474 washed with 2 × 1 mL cell lysis buffer, 1mL 1 M KCl, 1 mL 0.1 M Na_2CO_3, 1 mL of 2 M urea in 10 mM Tris-
475 HCl (pH 8.0), and again with 2 × 1 mL cell lysis buffer. Biotinylated proteins were then eluted by boiling the
476 magnetic beads in 30 µL 4 × Laemmli sample buffer (Bio-Rad, Cat.# 1610747) supplemented with 20 mM
477 DTT and 2 mM biotin.
478
479 **LC-MS/MS and label-free quantitative mass spectrometry proteomic analysis**
480 The streptavidin-enriched proteins were profiled using label-free quantitative mass spectrometry as
481 previously described (B. Zhou et al., 2019) at Cedars-Sinai Medical Center Biomarker Discovery Platform
482 Core.
483
484 **Data analysis for RNA proximal proteins**
485 Data were first filtered to exclude non-human proteins and proteins that were detected in only one or none
486 of the *U1* replicates or poly(A) replicates. Then proteins detected with two or greater unique peptides were
487 subjected to $\log_2$ transformation. Only the top gene name was kept from multiple candidates. Since *U1* has
488 compact structure in pre-B complex and its size is much smaller than the biotinylating range of APEX2,

489 experiments using *U1* gRNAs (*U1*-1, *U1*-2, *U1*-3) were considered as replicates to compare with
490 nontargeting controls (NTC1, partially [65%] targeting UBTF; NTC2, targeting poly[A]; NTC3, targeting
491 poly[U]). Moderated *t*-test with a paired design was used to compare the $\log_2$-transformed iBAQ values
492 between *U1* and NTC or between poly(A) and poly(U) using limma package (***Smyth, 2004***). *p* values were
493 adjust using the Benjamini-Hochberg (BH) method (***Benjamini and Hochberg, 1995***) for multiple
494 comparisons. Proteins with $p < 0.05$ were considered statistically significant. There are 226 *U1* RPPs with
495 $p < 0.05$, $\log_2$FC > 2, FDR < 0.25 and 786 poly(A) tail RPPs with BH-adjusted $p < 0.05$, $\log_2$FC > 2.
496
497 **Comparison RPPs with different gene ontology (GO) terms**
498 Lists of human proteins were retrieved (04/13/2020) from QuickGO (https://www.ebi.ac.uk/QuickGO/) *via*
499 searching corresponding GO terms and selecting '*Homo sapiens (9606)*' under Taxon, except P-bodies
500 and stress granule, which were both curated using data summarized from Wikipedia (04/24/2020)
501 (https://en.wikipedia.org/wiki/P-bodies, https://en.wikipedia.org/wiki/Stress_granule). The venn diagrams
502 were generated using online tools (http://bioinformatics.psb.ugent.be/webtools/Venn/).
503
504 **Cellular fractionation.** Cells were fractionated as previously described with slight modification (***Lin et al.,***
505 ***2019***). Six million HEK293T cells were treated with PML buffer (10 mM Tris-HCl, pH 7.5, 0.15% NP-40, 150
506 mM NaCl) on ice for 4 min after homogenization by flicking. Lysates were loaded onto a 24% sucrose
507 cushion (24% RNase-free sucrose in PML buffer) using large orifice tips, and centrifuged at 15,000 × *g* for
508 10 min at 4°C. The supernatant (cytoplasmic fraction) was retained and the pellet (nuclear fraction) was
509 washed with 1 × PBS/1 mM EDTA and resuspended in 200 µL of 1 × PBS/1 mM EDTA. Fractionation
510 efficiency was validated by western blot using β-tubulin (Sigma Aldrich, Cat.# T8328, 1:2,000) as
511 cytoplasmic marker and U1-70k (EMD Millipore, Cat.# 05-1588, 1:1,000) as nuclear marker.
512
513 **RNA Immunoprecipitation (RIP).** RIP was performed as previously described with slight modification (***Lin***
514 ***et al., 2019***). Twelve microliter Dynabeads Protein A (Thermo Fisher Scientific, Cat.#: 10001D) were
515 washed with 200 µL HBS (150 mM NaCl, 10 mM HEPES, pH7.5 by KOH) and incubated with 2 µg anti-HA
516 (Santa Cruz, Cat.# sc-7392) or 2 µg rabbit IgG isotype (Thermo Fisher Scientific, Cat.# 10500C) in the

517 presence of 80 μL HBS buffer at room temperature for 1 h. Eight million HEK293T cells were lysed with
518 800 μL cell lysis buffer (HBS, 0.1% NP-40, 5 mM EGTA, supplemented with 1 × protease inhibitor cocktail
519 [Roche, Cat.# 11873580001], 1 × PhosSTOP protease inhibitor cocktail [Roche, Cat.# 4906837001], 1 mM
520 PMSF [Sigma Aldrich, Cat.# 93482], and Superase-in [Ambion, Cat.# AM2696]) at 4°C for 1 h. Cell debris
521 and insoluble proteins were removed by centrifugation at 4°C, 12,000 *g* for 10 min, and the supernatants
522 were incubated with HA-conjugated or IgG-conjugated Dynabeads at 4°C for 1 h. The Dynabeads were
523 then washed 3 times with wash buffer (HBS, 0.1% NP-40) and aliquoted into two halves. Proteins
524 associated with half of the Dynabeads were eluted with 22 μL 4 × Laemmli sample buffer (Bio-Rad, Cat.#
525 1610747) by boiling at 95 °C for 5 min. RNA was extracted from the other half of Dynabeads using TRIzol
526 LS (Thermo Fisher Scientific, Cat.# 10296028).
527
528 **RNA extraction and RT-qPCR.** RNA associated with immunoprecipitated RPL fusion protein or RNA from
529 gRNA transfected cells were extracted using TRIzol LS. M-MLV reverse transcriptase (Promega, Cat.#
530 M5301) and random hexamers (Promega, Cat.# C1181) were used for reverse transcription. Gene
531 expression was quantified by RT-qPCR using iQ SYBR Green supermix (Bio-Rad, Cat.# 170-8886). The
532 relative gene expression was calculated using the $2^{-\Delta\Delta Ct}$ method and normalized to GAPDH. Five
533 nanograms cDNA was used for RT-qPCR analysis on CFX96 Touch Real-Time PCR Detection System
534 (Bio-Rad) using the following primer pairs:
535 U1-RT-For: 5'CCAGGGCGAGGCTTATCCATT3', U1-RT-Rev: 5'GCAGTCCCCCACTACCACAAAT3';
536 U2-RT-For: TTCTCGGCCTTTTGGCTAAG; U2-RT-Rev: CTCCCTGCTCCAAAAATCCA;
537 U6-RT-For: GCTTCGGCAGCACATATACTAAAAT; U6-RT-Rev: CGCTTCACGAATTTGCGTGTCAT;
538 5.8S-RT-For: GGTGGATCACTCGGCTCGT; 5.8S-RT-Rev: GCAAGTGCGTTCGAAGTGTC;
539 18S-RT-For: 5'CAGCCACCCGAGATTGAGCA3', 18S-RT-Rev: 5'TAGTAGCGACGGGCGTGTG3';
540 28S-RT-For: CCCAGTGCTCTGAATGTCAA; 28S-RT-Rev: AGTGGGAATCTCGTTCATCC;
541 GAPDH-RT-For: 5'TGCCAAATATGATGACATCAAGAA3',
542 GAPDH-RT-Rev: 5'GGAGTGGGTGTCGCTGTTG3'.
543

544 **Western blot.** Protein samples were run on 4-20% gradient precast protein gel (Bio-Rad, Cat.# 456-1096)
545 and transferred onto PVDF membrane (Bio-Rad, Cat.# 1704157). After 1 h blocking, membranes were
546 incubated with anti-FLAG (Santa Cruz, Cat.# sc-166384, 1:1,000), anti-HA (Santa Cruz, Cat.# sc-7392,
547 1:1,000), anti-biotin (Santa Cruz, Cat.# sc-57636, 1:1,000), or anti- β-actin (Santa Cruz, Cat.# sc-47778,
548 1:2,000) at 4°C overnight. Membranes were washed three times with Tris-buffered saline containing 0.5%
549 Tween 20 (TBST) before incubating with HRP-conjugated secondary antibody at room temperature for 2 h.
550 Then the membranes were incubated briefly with ECL Western Blotting Substrate (Thermo Fisher Scientific,
551 Cat.#: 32106) after three times wash with TBST. The membranes were exposed to HyBlot Autoradiography
552 Film (Denville Scientific, Cat.#: E3018).
553
554 **Distance calculation.** The distances between *U1* snRNA and *U1* RPPs identified by RPL in the pre-B
555 complex structure (PDB ID: 6QX9) were measured using PyMOL (***Schrodinger, 2020***). We used the
556 distance from *U1* snRNA (nucleotide 1) to the proximal residues of *U1* RPPs to estimate the actual distance
557 (D1). Since there is no structure available for PspCas13b, we used the structure of PbuCas13b (PDB ID:
558 6DTD) to infer the distance between *U1* RPPs and APEX2 in the RPL protein. Basically, the average
559 distances between gRNA (nucleotide 1, 12, and 23 of spacer) and the C-terminus of PbuCas13b, where
560 the APEX2 was fused to, were measured (D2). The inferred distances between APEX2 and RPPs were
561 then calculated as absolute value of the differences between D1 and D2.
562
563 **Data availability.** Raw images for western blots and raw mass spectrometry data for both *U1* RPPs and
564 poly(A) RPPs are included as supporting files.
565

566 **References**

567 Abudayyeh OO, Gootenberg JS, Essletzbichler P, Han S, Joung J, Belanto JJ, Verdine V, Cox DBT, Kellner
568 MJ, Regev A, Lander ES, Voytas DF, Ting AY, Zhang F. 2017. RNA targeting with CRISPR-Cas13.
569 *Nature* **550**:280–284. doi:10.1038/nature24049
570 Baltz AG, Munschauer M, Schwanhäusser B, Vasile A, Murakawa Y, Schueler M, Youngs N, Penfold-Brown
571 D, Drew K, Milek M, Wyler E, Bonneau R, Selbach M, Dieterich C, Landthaler M. 2012. The mRNA-
572 Bound Proteome and Its Global Occupancy Profile on Protein-Coding Transcripts. *Molecular Cell*
573 **46**:674–690. doi:10.1016/j.molcel.2012.05.021
574 Bandaru S, Tsuji MH, Shimizu Y, Usami K, Lee S, Takei NK, Yoshitome K, Nishimura Y, Otsuki T, Ito T.
575 2020. Structure-based design of gRNA for Cas13. *Sci Rep* **10**:11610. doi:10.1038/s41598-020-
576 68459-4
577 Batista PJ, Chang HY. 2013. Long Noncoding RNAs: Cellular Address Codes in Development and Disease.
578 *Cell* **152**:1298–1307. doi:10.1016/j.cell.2013.02.012
579 Belousov VV, Fradkov AF, Lukyanov KA, Staroverov DB, Shakhbazov KS, Terskikh AV, Lukyanov S. 2006.
580 Genetically encoded fluorescent indicator for intracellular hydrogen peroxide. *Nat Methods* **3**:281–
581 286. doi:10.1038/nmeth866
582 Benjamini Y, Hochberg Y. 1995. Controlling the False Discovery Rate: A Practical and Powerful Approach
583 to Multiple Testing. *Journal of the Royal Statistical Society: Series B (Methodological)* **57**:289–300.
584 doi:10.1111/j.2517-6161.1995.tb02031.x
585 Bernard JJ, Cowing-Zitron C, Nakatsuji T, Muehleisen B, Muto J, Borkowski AW, Martinez L, Greidinger
586 EL, Yu BD, Gallo RL. 2012. Ultraviolet radiation damages self noncoding RNA and is detected by
587 TLR3. *Nat Med* **18**:1286–1290. doi:10.1038/nm.2861
588 Berretta J, Morillon A. 2009. Pervasive transcription constitutes a new level of eukaryotic genome regulation.
589 *EMBO Rep* **10**:973–982. doi:10.1038/embor.2009.181
590 Blower MD. 2013. Molecular Insights into Intracellular RNA LocalizationInternational Review of Cell and
591 Molecular Biology. Elsevier. pp. 1–39. doi:10.1016/B978-0-12-407699-0.00001-7
592 Bohnsack MT, Czaplinski K, Gorlich D. 2004. Exportin 5 is a RanGTP-dependent dsRNA-binding protein
593 that mediates nuclear export of pre-miRNAs. *RNA* **10**:185–191. doi:10.1261/rna.5167604
594 Branon T, Han S, Ting A. 2017. Beyond Immunoprecipitation: Exploring New Interaction Spaces with
595 Proximity Biotinylation. *Biochemistry* **56**:3297–3298. doi:10.1021/acs.biochem.7b00466
596 Branon TC, Bosch JA, Sanchez AD, Udeshi ND, Svinkina T, Carr SA, Feldman JL, Perrimon N, Ting AY.
597 2018. Efficient proximity labeling in living cells and organisms with TurboID. *Nat Biotechnol* **36**:880–
598 887. doi:10.1038/nbt.4201
599 Cai X. 2004. Human microRNAs are processed from capped, polyadenylated transcripts that can also
600 function as mRNAs. *RNA* **10**:1957–1966. doi:10.1261/rna.7135204
601 Carlevaro-Fita J, Johnson R. 2019. Global Positioning System: Understanding Long Noncoding RNAs
602 through Subcellular Localization. *Mol Cell* **73**:869–883. doi:10.1016/j.molcel.2019.02.008
603 Castello A, Fischer B, Eichelbaum K, Horos R, Beckmann BM, Strein C, Davey NE, Humphreys DT, Preiss
604 T, Steinmetz LM, Krijgsveld J, Hentze MW. 2012. Insights into RNA biology from an atlas of
605 mammalian mRNA-binding proteins. *Cell* **149**:1393–1406. doi:10.1016/j.cell.2012.04.031
606 Caudron-Herger M, Rusin SF, Adamo ME, Seiler J, Schmid VK, Barreau E, Kettenbach AN, Diederichs S.
607 2019. R-DeeP: Proteome-wide and Quantitative Identification of RNA-Dependent Proteins by
608 Density Gradient Ultracentrifugation. *Mol Cell* **75**:184-199.e10. doi:10.1016/j.molcel.2019.04.018
609 Chang H, Lim J, Ha M, Kim VN. 2014. TAIL-seq: Genome-wide Determination of Poly(A) Tail Length and
610 3′ End Modifications. *Molecular Cell* **53**:1044–1052. doi:10.1016/j.molcel.2014.02.007
611 Chang Y-F, Imam JS, Wilkinson MF. 2007. The Nonsense-Mediated Decay RNA Surveillance Pathway.
612 *Annu Rev Biochem* **76**:51–74. doi:10.1146/annurev.biochem.76.050106.093909
613 Charenton C, Wilkinson ME, Nagai K. 2019. Mechanism of 5' splice site transfer for human spliceosome
614 activation. *Science* **364**:362–367. doi:10.1126/science.aax3289
615 Chen C-YA, Shyu A-B. 2011. Mechanisms of deadenylation-dependent decay: Mechanisms of
616 deadenylation-dependent decay. *WIREs RNA* **2**:167–183. doi:10.1002/wrna.40
617 Chlebowski A, Lubas M, Jensen TH, Dziembowski A. 2013. RNA decay machines: The exosome.
618 *Biochimica et Biophysica Acta (BBA) - Gene Regulatory Mechanisms* **1829**:552–560.
619 doi:10.1016/j.bbagrm.2013.01.006

620 Chu Ci, Spitale RC, Chang HY. 2015. Technologies to probe functions and mechanisms of long noncoding
621 RNAs. *Nat Struct Mol Biol* **22**:29–35. doi:10.1038/nsmb.2921
622 Chu C., Zhang QC, da Rocha ST, Flynn RA, Bharadwaj M, Calabrese JM, Magnuson T, Heard E, Chang
623 HY. 2015. Systematic discovery of Xist RNA binding proteins. *Cell* **161**:404–16.
624 doi:10.1016/j.cell.2015.03.025
625 Cioni J-M, Lin JQ, Holtermann AV, Koppers M, Jakobs MAH, Azizi A, Turner-Bridger B, Shigeoka T, Franze
626 K, Harris WA, Holt CE. 2019. Late Endosomes Act as mRNA Translation Platforms and Sustain
627 Mitochondria in Axons. *Cell* **176**:56-72.e15. doi:10.1016/j.cell.2018.11.030
628 Clément M-V, Pervaiz S. 2001. Intracellular superoxide and hydrogen peroxide concentrations: a critical
629 balance that determines survival or death. *Redox Report* **6**:211–214.
630 doi:10.1179/135100001101536346
631 Collart MA. 2016. The Ccr4-Not complex is a key regulator of eukaryotic gene expression. *Wiley Interdiscip*
632 *Rev RNA* **7**:438–454. doi:10.1002/wrna.1332
633 Cox DBT, Gootenberg JS, Abudayyeh OO, Franklin B, Kellner MJ, Joung J, Zhang F. 2017. RNA editing
634 with CRISPR-Cas13. *Science* **358**:1019–1027. doi:10.1126/science.aaq0180
635 Cvitkovic I, Jurica MS. 2013. Spliceosome database: a tool for tracking components of the spliceosome.
636 *Nucleic Acids Res* **41**:D132-141. doi:10.1093/nar/gks999
637 Damgaard CK, Kahns S, Lykke-Andersen S, Nielsen AL, Jensen TH, Kjems J. 2008. A 5′ Splice Site
638 Enhances the Recruitment of Basal Transcription Initiation Factors In Vivo. *Molecular Cell* **29**:271–
639 278. doi:10.1016/j.molcel.2007.11.035
640 Decker CJ, Parker R. 2012. P-Bodies and Stress Granules: Possible Roles in the Control of Translation
641 and mRNA Degradation. *Cold Spring Harbor Perspectives in Biology* **4**:a012286–a012286.
642 doi:10.1101/cshperspect.a012286
643 Deckert J, Hartmuth K, Boehringer D, Behzadnia N, Will CL, Kastner B, Stark H, Urlaub H, Lührmann R.
644 2006. Protein Composition and Electron Microscopy Structure of Affinity-Purified Human
645 Spliceosomal B Complexes Isolated under Physiological Conditions. *MCB* **26**:5528–5543.
646 doi:10.1128/MCB.00582-06
647 Derrien T, Johnson R, Bussotti G, Tanzer A, Djebali S, Tilgner H, Guernec G, Martin D, Merkel A, Knowles
648 DG, Lagarde J, Veeravalli L, Ruan X, Ruan Y, Lassmann T, Carninci P, Brown JB, Lipovich L,
649 Gonzalez JM, Thomas M, Davis CA, Shiekhattar R, Gingeras TR, Hubbard TJ, Notredame C,
650 Harrow J, Guigó R. 2012. The GENCODE v7 catalog of human long noncoding RNAs: analysis of
651 their gene structure, evolution, and expression. *Genome Res* **22**:1775–89.
652 doi:10.1101/gr.132159.111
653 Djebali S, Davis CA, Merkel A, Dobin A, Lassmann T, Mortazavi A, Tanzer A, Lagarde J, Lin W, Schlesinger
654 F, Xue C, Marinov GK, Khatun J, Williams BA, Zaleski C, Rozowsky J, Röder M, Kokocinski F,
655 Abdelhamid RF, Alioto T, Antoshechkin I, Baer MT, Bar NS, Batut P, Bell K, Bell I, Chakrabortty S,
656 Chen X, Chrast J, Curado J, Derrien T, Drenkow J, Dumais E, Dumais J, Duttagupta R, Falconnet
657 E, Fastuca M, Fejes-Toth K, Ferreira P, Foissac S, Fullwood MJ, Gao H, Gonzalez D, Gordon A,
658 Gunawardena H, Howald C, Jha S, Johnson R, Kapranov P, King B, Kingswood C, Luo OJ, Park
659 E, Persaud K, Preall JB, Ribeca P, Risk B, Robyr D, Sammeth M, Schaffer L, See LH, Shahab A,
660 Skancke J, Suzuki AM, Takahashi H, Tilgner H, Trout D, Walters N, Wang H, Wrobel J, Yu Y, Ruan
661 X, Hayashizaki Y, Harrow J, Gerstein M, Hubbard T, Reymond A, Antonarakis SE, Hannon G,
662 Giddings MC, Ruan Y, Wold B, Carninci P, Guigó R, Gingeras TR. 2012. Landscape of transcription
663 in human cells. *Nature* **489**:101–8. doi:10.1038/nature11233
664 Dreyfus M, Régnier P. 2002. The Poly(A) Tail of mRNAs. *Cell* **111**:611–613. doi:10.1016/S0092-
665 8674(02)01137-6
666 Dreyfuss G, Kim VN, Kataoka N. 2002. Messenger-RNA-binding proteins and the messages they carry.
667 *Nat Rev Mol Cell Biol* **3**:195–205. doi:10.1038/nrm760
668 ElMaghraby MF, Andersen PR, Pühringer F, Hohmann U, Meixner K, Lendl T, Tirian L, Brennecke J. 2019.
669 A Heterochromatin-Specific RNA Export Pathway Facilitates piRNA Production. *Cell* **178**:964-
670 979.e20. doi:10.1016/j.cell.2019.07.007
671 Engreitz JM, Sirokman K, McDonel P, Shishkin AA, Surka C, Russell P, Grossman SR, Chow AY, Guttman
672 M, Lander ES. 2014. RNA-RNA Interactions Enable Specific Targeting of Noncoding RNAs to
673 Nascent Pre-mRNAs and Chromatin Sites. *Cell* **159**:188–199. doi:10.1016/j.cell.2014.08.018
674 Fazal FM, Han S, Parker KR, Kaewsapsak P, Xu J, Boettiger AN, Chang HY, Ting AY. 2019. Atlas of
675 Subcellular RNA Localization Revealed by APEX-Seq. *Cell*. doi:10.1016/j.cell.2019.05.027

676 Fujiwara Y, Furuta A, Kikuchi H, Aizawa S, Hatanaka Y, Konya C, Uchida K, Yoshimura A, Tamai Y, Wada
677 K, Kabuta T. 2013. Discovery of a novel type of autophagy targeting RNA. *Autophagy* **9**:403–409.
678 doi:10.4161/auto.23002
679 Gesteland RF. 1993. The RNA world: the nature of modern RNA suggests a prebiotic RNA world. New
680 York: Cold Spring Harbor Laboratory Press.
681 Ghildiyal M, Zamore PD. 2009. Small silencing RNAs: an expanding universe. *Nat Rev Genet* **10**:94–108.
682 doi:10.1038/nrg2504
683 Gilmartin GM. 2005. Eukaryotic mRNA 3' processing: a common means to different ends. *Genes Dev*
684 **19**:2517–2521. doi:10.1101/gad.1378105
685 Glisovic T, Bachorik JL, Yong J, Dreyfuss G. 2008. RNA-binding proteins and post-transcriptional gene
686 regulation. *FEBS Lett* **582**:1977–1986. doi:10.1016/j.febslet.2008.03.004
687 Gootenberg JS, Abudayyeh OO, Kellner MJ, Joung J, Collins JJ, Zhang F. 2018. Multiplexed and portable
688 nucleic acid detection platform with Cas13, Cas12a, and Csm6. *Science* **360**:439–444.
689 doi:10.1126/science.aaq0179
690 Graindorge A, Pinheiro I, Nawrocka A, Mallory AC, Tsvetkov P, Gil N, Carolis C, Buchholz F, Ulitsky I,
691 Heard E, Taipale M, Shkumatava A. 2019. In-cell identification and measurement of RNA-protein
692 interactions. *Nat Commun* **10**:5317. doi:10.1038/s41467-019-13235-w
693 Guttman M, Amit I, Garber M, French C, Lin MF, Feldser D, Huarte M, Zuk O, Carey BW, Cassady JP,
694 Cabili MN, Jaenisch R, Mikkelsen TS, Jacks T, Hacohen N, Bernstein BE, Kellis M, Regev A, Rinn
695 JL, Lander ES. 2009. Chromatin signature reveals over a thousand highly conserved large non-
696 coding RNAs in mammals. *Nature* **458**:223–7. doi:10.1038/nature07672
697 Han S, Zhao BS, Myers SA, Carr SA, He C, Ting AY. 2020. RNA–protein interaction mapping via MS2- or
698 Cas13-based APEX targeting. *Proc Natl Acad Sci USA* 202006617. doi:10.1073/pnas.2006617117
699 Hentze MW, Castello A, Schwarzl T, Preiss T. 2018. A brave new world of RNA-binding proteins. *Nat Rev*
700 *Mol Cell Biol* **19**:327–341. doi:10.1038/nrm.2017.130
701 Holt CE, Bullock SL. 2009. Subcellular mRNA Localization in Animal Cells and Why It Matters. *Science*
702 **326**:1212–1216. doi:10.1126/science.1176488
703 Huang BK, Sikes HD. 2014. Quantifying intracellular hydrogen peroxide perturbations in terms of
704 concentration. *Redox Biology* **2**:955–962. doi:10.1016/j.redox.2014.08.001
705 Huang Y, Carmichael GG. 1996. Role of polyadenylation in nucleocytoplasmic transport of mRNA. *Mol Cell*
706 *Biol* **16**:1534–1542. doi:10.1128/MCB.16.4.1534
707 Huang Y, Guo Q, Ding X-P, Wang X. 2020. Mechanism of long noncoding RNAs as transcriptional
708 regulators in cancer. *RNA Biology* 1–13. doi:10.1080/15476286.2019.1710405
709 International Human Genome Sequencing Consortium. 2001. Initial sequencing and analysis of the human
710 genome. *Nature* **409**:860–921. doi:10.1038/35057062
711 Iyer MK, Niknafs YS, Malik R, Singhal U, Sahu A, Hosono Y, Barrette TR, Prensner JR, Evans JR, Zhao S,
712 Poliakov A, Cao X, Dhanasekaran SM, Wu Y-M, Robinson DR, Beer DG, Feng FY, Iyer HK,
713 Chinnaiyan AM. 2015. The landscape of long noncoding RNAs in the human transcriptome. *Nat*
714 *Genet* **47**:199–208. doi:10.1038/ng.3192
715 Kadaba S, Wang X, Anderson JT. 2006. Nuclear RNA surveillance in Saccharomyces cerevisiae: Trf4p-
716 dependent polyadenylation of nascent hypomethylated tRNA and an aberrant form of 5S rRNA.
717 *RNA* **12**:508–521. doi:10.1261/rna.2305406
718 Kim DI, Jensen SC, Noble KA, Kc B, Roux KH, Motamedchaboki K, Roux KJ. 2016. An improved smaller
719 biotin ligase for BioID proximity labeling. *MBoC* **27**:1188–1196. doi:10.1091/mbc.E15-12-0844
720 Kim VN. 2005. MicroRNA biogenesis: coordinated cropping and dicing. *Nat Rev Mol Cell Biol* **6**:376–385.
721 doi:10.1038/nrm1644
722 Kneuss E, Munafò M, Eastwood EL, Deumer U-S, Preall JB, Hannon GJ, Czech B. 2019. Specialization of
723 the Drosophila nuclear export family protein Nxf3 for piRNA precursor export. *Genes Dev* **33**:1208–
724 1220. doi:10.1101/gad.328690.119
725 Köhler A, Hurt E. 2007. Exporting RNA from the nucleus to the cytoplasm. *Nat Rev Mol Cell Biol* **8**:761–
726 773. doi:10.1038/nrm2255
727 Konermann S, Lotfy P, Brideau NJ, Oki J, Shokhirev MN, Hsu PD. 2018. Transcriptome Engineering with
728 RNA-Targeting Type VI-D CRISPR Effectors. *Cell* **173**:665-676.e14.
729 doi:10.1016/j.cell.2018.02.033
730 Kopp F, Mendell JT. 2018. Functional Classification and Experimental Dissection of Long Noncoding RNAs.
731 *Cell* **172**:393–407. doi:10.1016/j.cell.2018.01.011

732 Kruse C, Willkomm DK, Grünweller A, Vollbrandt T, Sommer S, Busch S, Pfeiffer T, Brinkmann J, Hartmann
733 RK, Müller PK. 2000. Export and transport of tRNA are coupled to a multi-protein complex. *Biochem*
734 *J* **346 Pt 1**:107–115.
735 Kwek KY, Murphy S, Furger A, Thomas B, O'Gorman W, Kimura H, Proudfoot NJ, Akoulitchev A. 2002. U1
736 snRNA associates with TFIIH and regulates transcriptional initiation. *Nat Struct Biol*.
737 doi:10.1038/nsb862
738 Kwon SC, Yi H, Eichelbaum K, Föhr S, Fischer B, You KT, Castello A, Krijgsveld J, Hentze MW, Kim VN.
739 2013. The RNA-binding protein repertoire of embryonic stem cells. *Nat Struct Mol Biol* **20**:1122–
740 1130. doi:10.1038/nsmb.2638
741 Lai W-JC, Kayedkhordeh M, Cornell EV, Farah E, Bellaousov S, Rietmeijer R, Salsi E, Mathews DH,
742 Ermolenko DN. 2018. mRNAs and lncRNAs intrinsically form secondary structures with short end-
743 to-end distances. *Nat Commun* **9**:4328. doi:10.1038/s41467-018-06792-z
744 Lam SS, Martell JD, Kamer KJ, Deerinck TJ, Ellisman MH, Mootha VK, Ting AY. 2015. Directed evolution
745 of APEX2 for electron microscopy and proximity labeling. *Nat Methods* **12**:51–54.
746 doi:10.1038/nmeth.3179
747 Laprade H, Querido E, Smith MJ, Guérit D, Crimmins H, Conomos D, Pourret E, Chartrand P, Sfeir A. 2020.
748 Single-Molecule Imaging of Telomerase RNA Reveals a Recruitment-Retention Model for
749 Telomere Elongation. *Molecular Cell* **79**:115-126.e6. doi:10.1016/j.molcel.2020.05.005
750 Laroia G, Cuesta R, Brewer G, Schneider RJ. 1999. Control of mRNA decay by heat shock-ubiquitin-
751 proteasome pathway. *Science* **284**:499–502. doi:10.1126/science.284.5413.499
752 Laroia G, Sarkar B, Schneider RJ. 2002. Ubiquitin-dependent mechanism regulates rapid turnover of AU-
753 rich cytokine mRNAs. *Proc Natl Acad Sci USA* **99**:1842–1846. doi:10.1073/pnas.042575699
754 Lebbink RJ, Lowe M, Chan T, Khine H, Wang X, McManus MT. 2011. Polymerase II promoter strength
755 determines efficacy of microRNA adapted shRNAs. *PLoS ONE* **6**:e26213.
756 doi:10.1371/journal.pone.0026213
757 Leija-Martínez N, Casas-Flores S, Cadena-Nava RD, Roca JA, Mendez-Cabañas JA, Gomez E, Ruiz-
758 Garcia J. 2014. The separation between the 5′-3′ ends in long RNA molecules is short and nearly
759 constant. *Nucleic Acids Research* **42**:13963–13968. doi:10.1093/nar/gku1249
760 Lemmens I, Jansen S, de Rouck S, de Smet A-S, Defever D, Neyts J, Dallmeier K, Tavernier J. 2020. The
761 Development of RNA-KISS, a Mammalian Three-Hybrid Method to Detect RNA–Protein
762 Interactions in Living Mammalian Cells. *J Proteome Res* acs.jproteome.0c00068.
763 doi:10.1021/acs.jproteome.0c00068
764 Li J-H, Liu S, Zhou H, Qu L-H, Yang J-H. 2014. starBase v2.0: decoding miRNA-ceRNA, miRNA-ncRNA
765 and protein–RNA interaction networks from large-scale CLIP-Seq data. *Nucl Acids Res* **42**:D92–
766 D97. doi:10.1093/nar/gkt1248
767 Li X, Fu X-D. 2019. Chromatin-associated RNAs as facilitators of functional genomic interactions. *Nat Rev*
768 *Genet*. doi:10.1038/s41576-019-0135-1
769 Li XZ, Roy CK, Dong X, Bolcun-Filas E, Wang J, Han BW, Xu J, Moore MJ, Schimenti JC, Weng Z, Zamore
770 PD. 2013. An ancient transcription factor initiates the burst of piRNA production during early
771 meiosis in mouse testes. *Mol Cell* **50**:67–81. doi:10.1016/j.molcel.2013.02.016
772 Li Y, Liu S, Cao L, Luo Y, Du H, Li S, You F. 2020. CBRPP: a new RNA-centric method to study RNA-
773 protein interactions (preprint). Molecular Biology. doi:10.1101/2020.04.09.033290
774 Licatalosi DD, Mele A, Fak JJ, Ule J, Kayikci M, Chi SW, Clark TA, Schweitzer AC, Blume JE, Wang X,
775 Darnell JC, Darnell RB. 2008. HITS-CLIP yields genome-wide insights into brain alternative RNA
776 processing. *Nature* **456**:464–469. doi:10.1038/nature07488
777 Lim J, Kim D, Lee Y, Ha M, Lee M, Yeo J, Chang H, Song J, Ahn K, Kim VN. 2018. Mixed tailing by TENT4A
778 and TENT4B shields mRNA from rapid deadenylation. *Science* **361**:701–704.
779 doi:10.1126/science.aam5794
780 Lin X, Spindler TJ, de Souza Fonseca MA, Corona RI, Seo J-H, Dezem FS, Li L, Lee JM, Long HW, Sellers
781 TA, Karlan BY, Noushmehr H, Freedman ML, Gayther SA, Lawrenson K. 2019. Super-Enhancer-
782 Associated LncRNA UCA1 Interacts Directly with AMOT to Activate YAP Target Genes in Epithelial
783 Ovarian Cancer. *iScience* **17**:242–255. doi:10.1016/j.isci.2019.06.025
784 Liu Q, Zheng J, Sun W, Huo Y, Zhang L, Hao P, Wang H, Zhuang M. 2018. A proximity-tagging system to
785 identify membrane protein–protein interactions. *Nat Methods* **15**:715–722. doi:10.1038/s41592-
786 018-0100-5

Lund E, Güttinger S, Calado A, Dahlberg JE, Kutay U. 2004. Nuclear export of microRNA precursors. *Science* **303**:95–98. doi:10.1126/science.1090599

Lunde BM, Moore C, Varani G. 2007. RNA-binding proteins: modular design for efficient function. *Nat Rev Mol Cell Biol* **8**:479–490. doi:10.1038/nrm2178

Lyublinskaya O, Antunes F. 2019. Measuring intracellular concentration of hydrogen peroxide with the use of genetically encoded H2O2 biosensor HyPer. *Redox Biology* **24**:101200. doi:10.1016/j.redox.2019.101200

Malone CD, Hannon GJ. 2009. Small RNAs as guardians of the genome. *Cell* **136**:656–668. doi:10.1016/j.cell.2009.01.045

McHugh CA, Chen CK, Chow A, Surka CF, Tran C, McDonel P, Pandya-Jones A, Blanco M, Burghard C, Moradian A, Sweredoski MJ, Shishkin AA, Su J, Lander ES, Hess S, Plath K, Guttman M. 2015. The Xist lncRNA interacts directly with SHARP to silence transcription through HDAC3. *Nature* **521**:232–6. doi:10.1038/nature14443

Metkar M, Ozadam H, Lajoie BR, Imakaev M, Mirny LA, Dekker J, Moore MJ. 2018. Higher-Order Organization Principles of Pre-translational mRNPs. *Molecular Cell* **72**:715-726.e3. doi:10.1016/j.molcel.2018.09.012

Milek M, Imami K, Mukherjee N, Bortoli FD, Zinnall U, Hazapis O, Trahan C, Oeffinger M, Heyd F, Ohler U, Selbach M, Landthaler M. 2017. DDX54 regulates transcriptome dynamics during DNA damage response. *Genome Res* **27**:1344–1359. doi:10.1101/gr.218438.116

Mofatteh M, Bullock SL. 2017. SnapShot: Subcellular mRNA Localization. *Cell* **169**:178-178.e1. doi:10.1016/j.cell.2017.03.004

Mugridge JS, Coller J, Gross JD. 2018. Structural and molecular mechanisms for the control of eukaryotic 5′–3′ mRNA decay. *Nat Struct Mol Biol* **25**:1077–1085. doi:10.1038/s41594-018-0164-z

Muhlrad D, Decker CJ, Parker R. 1994. Deadenylation of the unstable mRNA encoded by the yeast MFA2 gene leads to decapping followed by 5'-->3' digestion of the transcript. *Genes Dev* **8**:855–866. doi:10.1101/gad.8.7.855

Mukherjee J, Hermesh O, Eliscovich C, Nalpas N, Franz-Wachtel M, Maček B, Jansen R-P. 2019. β-Actin mRNA interactome mapping by proximity biotinylation. *Proc Natl Acad Sci USA* **116**:12863–12872. doi:10.1073/pnas.1820737116

Munro S. 2011. The Golgin Coiled-Coil Proteins of the Golgi Apparatus. *Cold Spring Harbor Perspectives in Biology* **3**:a005256–a005256. doi:10.1101/cshperspect.a005256

Norbury CJ. 2013. Cytoplasmic RNA: a case of the tail wagging the dog. *Nat Rev Mol Cell Biol* **14**:643–653. doi:10.1038/nrm3645

Okamura M, Inose H, Masuda S. 2015. RNA Export through the NPC in Eukaryotes. *Genes* **6**:124–149. doi:10.3390/genes6010124

Padrón A, Iwasaki S, Ingolia NT. 2019. Proximity RNA Labeling by APEX-Seq Reveals the Organization of Translation Initiation Complexes and Repressive RNA Granules. *Molecular Cell* **75**:875-887.e5. doi:10.1016/j.molcel.2019.07.030

Palacios I. 1997. Nuclear import of U snRNPs requires importin beta. *The EMBO Journal* **16**:6783–6792. doi:10.1093/emboj/16.22.6783

Panhale A, Richter FM, Ramírez F, Shvedunova M, Manke T, Mittler G, Akhtar A. 2019. CAPRI enables comparison of evolutionarily conserved RNA interacting regions. *Nat Commun* **10**:2682. doi:10.1038/s41467-019-10585-3

Pomeranz Krummel DA, Oubridge C, Leung AKW, Li J, Nagai K. 2009. Crystal structure of human spliceosomal U1 snRNP at 5.5 Å resolution. *Nature* **458**:475–480. doi:10.1038/nature07851

Queiroz RML, Smith T, Villanueva E, Marti-Solano M, Monti M, Pizzinga M, Mirea D-M, Ramakrishna M, Harvey RF, Dezi V, Thomas GH, Willis AE, Lilley KS. 2019. Comprehensive identification of RNA-protein interactions in any organism using orthogonal organic phase separation (OOPS). *Nat Biotechnol* **37**:169–178. doi:10.1038/s41587-018-0001-2

Quinn JJ, Ilik IA, Qu K, Georgiev P, Chu C, Akhtar A, Chang HY. 2014. Revealing long noncoding RNA architecture and functions using domain-specific chromatin isolation by RNA purification. *Nat Biotechnol* **32**:933–940. doi:10.1038/nbt.2943

Ramanathan M, Majzoub K, Rao DS, Neela PH, Zarnegar BJ, Mondal S, Roth JG, Gai H, Kovalski JR, Siprashvili Z, Palmer TD, Carette JE, Khavari PA. 2018. RNA-protein interaction detection in living cells. *Nat Methods* **15**:207–212. doi:10.1038/nmeth.4601

842 Ramanathan M, Porter DF, Khavari PA. 2019. Methods to study RNA-protein interactions. *Nat Methods*
843 **16**:225–234. doi:10.1038/s41592-019-0330-1
844 Rauch S, He E, Srienc M, Zhou H, Zhang Z, Dickinson BC. 2019. Programmable RNA-Guided RNA Effector
845 Proteins Built from Human Parts. *Cell* S0092867419306208. doi:10.1016/j.cell.2019.05.049
846 Rhee H-W, Zou P, Udeshi ND, Martell JD, Mootha VK, Carr SA, Ting AY. 2013. Proteomic Mapping of
847 Mitochondria in Living Cells via Spatially Restricted Enzymatic Tagging. *Science* **339**:1328–1331.
848 doi:10.1126/science.1230593
849 Roux KJ, Kim DI, Burke B. 2013. BioID: a screen for protein-protein interactions. *Curr Protoc Protein Sci*
850 **74**:19.23.1-19.23.14. doi:10.1002/0471140864.ps1923s74
851 Roux KJ, Kim DI, Raida M, Burke B. 2012. A promiscuous biotin ligase fusion protein identifies proximal
852 and interacting proteins in mammalian cells. *Journal of Cell Biology* **196**:801–810.
853 doi:10.1083/jcb.201112098
854 Samavarchi-Tehrani P, Samson R, Gingras A-C. 2020. Proximity Dependent Biotinylation: Key Enzymes
855 and Adaptation to Proteomics Approaches. *Mol Cell Proteomics* **19**:757–773.
856 doi:10.1074/mcp.R120.001941
857 Schrodinger. 2015. The PyMOL Molecular Graphics System, Version 1.8.
858 Shi Y, Manley JL. 2015. The end of the message: multiple protein–RNA interactions define the mRNA
859 polyadenylation site. *Genes Dev* **29**:889–897. doi:10.1101/gad.261974.115
860 Simon AE, Miller WA. 2013. 3' cap-independent translation enhancers of plant viruses. *Annu Rev Microbiol*
861 **67**:21–42. doi:10.1146/annurev-micro-092412-155609
862 Smargon AA, Cox DBT, Pyzocha NK, Zheng K, Slaymaker IM, Gootenberg JS, Abudayyeh OA,
863 Essletzbichler P, Shmakov S, Makarova KS, Koonin EV, Zhang F. 2017. Cas13b Is a Type VI-B
864 CRISPR-Associated RNA-Guided RNase Differentially Regulated by Accessory Proteins Csx27
865 and Csx28. *Mol Cell* **65**:618-630.e7. doi:10.1016/j.molcel.2016.12.023
866 Smyth GK. 2004. Linear Models and Empirical Bayes Methods for Assessing Differential Expression in
867 Microarray Experiments. *Statistical Applications in Genetics and Molecular Biology* **3**:1–25.
868 doi:10.2202/1544-6115.1027
869 So BR, Di C, Cai Z, Venters CC, Guo J, Oh J-M, Arai C, Dreyfuss G. 2019. A Complex of U1 snRNP with
870 Cleavage and Polyadenylation Factors Controls Telescripting, Regulating mRNA Transcription in
871 Human Cells. *Molecular Cell* **76**:590-599.e4. doi:10.1016/j.molcel.2019.08.007
872 Spiluttini B, Gu B, Belagal P, Smirnova AS, Nguyen VT, Hebert C, Schmidt U, Bertrand E, Darzacq X,
873 Bensaude O. 2010. Splicing-independent recruitment of U1 snRNP to a transcription unit in living
874 cells. *Journal of Cell Science* **123**:2085–2093. doi:10.1242/jcs.061358
875 Spitale RC, Flynn RA, Zhang QC, Crisalli P, Lee B, Jung J-W, Kuchelmeister HY, Batista PJ, Torre EA,
876 Kool ET, Chang HY. 2015. Structural imprints in vivo decode RNA regulatory mechanisms. *Nature*
877 **519**:486–490. doi:10.1038/nature14263
878 Stark H, Dube P, Lührmann R, Kastner B. 2001. Arrangement of RNA and proteins in the spliceosomal U1
879 small nuclear ribonucleoprotein particle. *Nature* **409**:539–542. doi:10.1038/35054102
880 Sun L, Fazal FM, Li P, Broughton JP, Lee B, Tang L, Huang W, Kool ET, Chang HY, Zhang QC. 2019.
881 RNA structure maps across mammalian cellular compartments. *Nat Struct Mol Biol* **26**:322–330.
882 doi:10.1038/s41594-019-0200-7
883 Szklarczyk D, Gable AL, Lyon D, Junge A, Wyder S, Huerta-Cepas J, Simonovic M, Doncheva NT, Morris
884 JH, Bork P, Jensen LJ, Mering C von. 2019. STRING v11: protein-protein association networks
885 with increased coverage, supporting functional discovery in genome-wide experimental datasets.
886 *Nucleic Acids Res* **47**:D607–D613. doi:10.1093/nar/gky1131
887 Tarn W-Y, Chang T-H. 2009. The current understanding of Ded1p/DDX3 homologs from yeast to human.
888 *RNA Biology* **6**:17–20. doi:10.4161/rna.6.1.7440
889 Tian B. 2005. A large-scale analysis of mRNA polyadenylation of human and mouse genes. *Nucleic Acids*
890 *Research* **33**:201–212. doi:10.1093/nar/gki158
891 Trendel J, Schwarzl T, Horos R, Prakash A, Bateman A, Hentze MW, Krijgsveld J. 2019. The Human RNA-
892 Binding Proteome and Its Dynamics during Translational Arrest. *Cell* **176**:391-403.e19.
893 doi:10.1016/j.cell.2018.11.004
894 Truniger V, Miras M, Aranda MA. 2017. Structural and Functional Diversity of Plant Virus 3'-Cap-
895 Independent Translation Enhancers (3'-CITEs). *Front Plant Sci* **8**:2047.
896 doi:10.3389/fpls.2017.02047

Urdaneta EC, Beckmann BM. 2019. Fast and unbiased purification of RNA-protein complexes after UV cross-linking. *Methods* S1046202318304869. doi:10.1016/j.ymeth.2019.09.013

Van Nostrand EL, Pratt GA, Shishkin AA, Gelboin-Burkhart C, Fang MY, Sundararaman B, Blue SM, Nguyen TB, Surka C, Elkins K, Stanton R, Rigo F, Guttman M, Yeo GW. 2016. Robust transcriptome-wide discovery of RNA-binding protein binding sites with enhanced CLIP (eCLIP). *Nat Methods* **13**:508–514. doi:10.1038/nmeth.3810

Venter JC, Adams MD, Myers EW, Li PW, Mural RJ, Sutton GG, Smith HO, Yandell M, Evans CA, Holt RA, Gocayne JD, Amanatides P, Ballew RM, Huson DH, Wortman JR, Zhang Q, Kodira CD, Zheng XH, Chen L, Skupski M, Subramanian G, Thomas PD, Zhang J, Gabor Miklos GL, Nelson C, Broder S, Clark AG, Nadeau J, McKusick VA, Zinder N, Levine AJ, Roberts RJ, Simon M, Slayman C, Hunkapiller M, Bolanos R, Delcher A, Dew I, Fasulo D, Flanigan M, Florea L, Halpern A, Hannenhalli S, Kravitz S, Levy S, Mobarry C, Reinert K, Remington K, Abu-Threideh J, Beasley E, Biddick K, Bonazzi V, Brandon R, Cargill M, Chandramouliswaran I, Charlab R, Chaturvedi K, Deng Z, Francesco VD, Dunn P, Eilbeck K, Evangelista C, Gabrielian AE, Gan W, Ge W, Gong F, Gu Z, Guan P, Heiman TJ, Higgins ME, Ji R-R, Ke Z, Ketchum KA, Lai Z, Lei Y, Li Z, Li J, Liang Y, Lin X, Lu F, Merkulov GV, Milshina N, Moore HM, Naik AK, Narayan VA, Neelam B, Nusskern D, Rusch DB, Salzberg S, Shao W, Shue B, Sun J, Wang ZY, Wang A, Wang X, Wang J, Wei M-H, Wides R, Xiao C, Yan C, Yao A, Ye J, Zhan M, Zhang W, Zhang H, Zhao Q, Zheng L, Zhong F, Zhong W, Zhu SC, Zhao S, Gilbert D, Baumhueter S, Spier G, Carter C, Cravchik A, Woodage T, Ali F, An H, Awe A, Baldwin D, Baden H, Barnstead M, Barrow I, Beeson K, Busam D, Carver A, Center A, Cheng ML, Curry L, Danaher S, Davenport L, Desilets R, Dietz S, Dodson K, Doup L, Ferriera S, Garg N, Gluecksmann A, Hart B, Haynes J, Haynes C, Heiner C, Hladun S, Hostin D, Houck J, Howland T, Ibegwam C, Johnson J, Kalush F, Kline L, Koduru S, Love A, Mann F, May D, McCawley S, McIntosh T, McMullen I, Moy M, Moy L, Murphy B, Nelson K, Pfannkoch C, Pratts E, Puri V, Qureshi H, Reardon M, Rodriguez R, Rogers Y-H, Romblad D, Ruhfel B, Scott R, Sitter C, Smallwood M, Stewart E, Strong R, Suh E, Thomas R, Tint NN, Tse S, Vech C, Wang G, Wetter J, Williams S, Williams M, Windsor S, Winn-Deen E, Wolfe K, Zaveri J, Zaveri K, Abril JF, Guigó R, Campbell MJ, Sjolander KV, Karlak B, Kejariwal A, Mi H, Lazareva B, Hatton T, Narechania A, Diemer K, Muruganujan A, Guo N, Sato S, Bafna V, Istrail S, Lippert R, Schwartz R, Walenz B, Yooseph S, Allen D, Basu A, Baxendale J, Blick L, Caminha M, Carnes-Stine J, Caulk P, Chiang Y-H, Coyne M, Dahlke C, Mays AD, Dombroski M, Donnelly M, Ely D, Esparham S, Fosler C, Gire H, Glanowski S, Glasser K, Glodek A, Gorokhov M, Graham K, Gropman B, Harris M, Heil J, Henderson S, Hoover J, Jennings D, Jordan C, Jordan J, Kasha J, Kagan L, Kraft C, Levitsky A, Lewis M, Liu X, Lopez J, Ma D, Majoros W, McDaniel J, Murphy S, Newman M, Nguyen T, Nguyen N, Nodell M, Pan S, Peck J, Peterson M, Rowe W, Sanders R, Scott J, Simpson M, Smith T, Sprague A, Stockwell T, Turner R, Venter E, Wang M, Wen M, Wu D, Wu M, Xia A, Zandieh A, Zhu X. 2001. The Sequence of the Human Genome. *Science* **291**:1304–1351. doi:10.1126/science.1058040

Weber G, Trowitzsch S, Kastner B, Lührmann R, Wahl MC. 2010. Functional organization of the Sm core in the crystal structure of human U1 snRNP. *EMBO J* **29**:4172–4184. doi:10.1038/emboj.2010.295

Wessels H-H, Méndez-Mancilla A, Guo X, Legut M, Daniloski Z, Sanjana NE. 2020. Massively parallel Cas13 screens reveal principles for guide RNA design. *Nat Biotechnol*. doi:10.1038/s41587-020-0456-9

Wilk R, Hu J, Blotsky D, Krause HM. 2016. Diverse and pervasive subcellular distributions for both coding and long noncoding RNAs. *Genes Dev* **30**:594–609. doi:10.1101/gad.276931.115

Wurtmann EJ, Wolin SL. 2009. RNA under attack: cellular handling of RNA damage. *Crit Rev Biochem Mol Biol* **44**:34–49. doi:10.1080/10409230802594043

Yamashita A, Chang T-C, Yamashita Y, Zhu W, Zhong Z, Chen C-YA, Shyu A-B. 2005. Concerted action of poly(A) nucleases and decapping enzyme in mammalian mRNA turnover. *Nat Struct Mol Biol* **12**:1054–1063. doi:10.1038/nsmb1016

Yan WX, Chong S, Zhang H, Makarova KS, Koonin EV, Cheng DR, Scott DA. 2018. Cas13d Is a Compact RNA-Targeting Type VI CRISPR Effector Positively Modulated by a WYL-Domain-Containing Accessory Protein. *Mol Cell* **70**:327-339.e5. doi:10.1016/j.molcel.2018.02.028

Yan Y-B. 2014. Deadenylation: enzymes, regulation, and functional implications: Regulation of deadenylation. *WIREs RNA* **5**:421–443. doi:10.1002/wrna.1221

952 Yang L, Duff MO, Graveley BR, Carmichael GG, Chen L-L. 2011. Genomewide characterization of non-
953 polyadenylated RNAs. *Genome Biol* **12**:R16. doi:10.1186/gb-2011-12-2-r16
954 Yang L, Froberg JE, Lee JT. 2014. Long noncoding RNAs: fresh perspectives into the RNA world. *Trends*
955 *in Biochemical Sciences* **39**:35–43. doi:10.1016/j.tibs.2013.10.002
956 Yang L-Z, Wang Y, Li S-Q, Yao R-W, Luan P-F, Wu H, Carmichael GG, Chen L-L. 2019. Dynamic Imaging
957 of RNA in Living Cells by CRISPR-Cas13 Systems. *Molecular Cell* **76**:981-997.e7.
958 doi:10.1016/j.molcel.2019.10.024
959 Yi R, Qin Y, Macara IG, Cullen BR. 2003. Exportin-5 mediates the nuclear export of pre-microRNAs and
960 short hairpin RNAs. *Genes Dev* **17**:3011–3016. doi:10.1101/gad.1158803
961 Yi W, Li J, Zhu X, Wang X, Fan L, Sun W, Liao L, Zhang J, Li X, Ye J, Chen F, Taipale J, Chan KM, Zhang
962 L, Yan J. 2020. CRISPR-assisted detection of RNA–protein interactions in living cells. *Nat Methods*.
963 doi:10.1038/s41592-020-0866-0
964 Yin Y, Lu JY, Zhang X, Shao W, Xu Y, Li P, Hong Y, Cui L, Shan G, Tian B, Zhang QC, Shen X. 2020. U1
965 snRNP regulates chromatin retention of noncoding RNAs. *Nature* **580**:147–150.
966 doi:10.1038/s41586-020-2105-3
967 Yu Y, Reed R. 2015. FUS functions in coupling transcription to splicing by mediating an interaction between
968 RNAP II and U1 snRNP. *Proc Natl Acad Sci USA* **112**:8608–8613. doi:10.1073/pnas.1506282112
969 Zhang C, Konermann S, Brideau NJ, Lotfy P, Wu X, Novick SJ, Strutzenberg T, Griffin PR, Hsu PD, Lyumkis
970 D. 2018. Structural Basis for the RNA-Guided Ribonuclease Activity of CRISPR-Cas13d. *Cell*
971 **175**:212-223.e17. doi:10.1016/j.cell.2018.09.001
972 Zhang Z, Sun W, Shi T, Lu P, Zhuang M, Liu J-L. 2020. Capturing RNA–protein interaction via CRUIS.
973 *Nucleic Acids Research* gkaa143. doi:10.1093/nar/gkaa143
974 Zhou B, Wang Y, Yan Y, Mariscal J, Di Vizio D, Freeman MR, Yang W. 2019. Low-Background Acyl-Biotinyl
975 Exchange Largely Eliminates the Coisolation of Non- *S* -Acylated Proteins and Enables Deep *S* -
976 Acylproteomic Analysis. *Anal Chem* **91**:9858–9866. doi:10.1021/acs.analchem.9b01520
977 Zhou Y, Wang G, Wang P, Li Z, Yue T, Wang J, Zou P. 2019. Expanding APEX2 Substrates for Proximity-
978 Dependent Labeling of Nucleic Acids and Proteins in Living Cells. *Angew Chem Int Ed* **58**:11763–
979 11767. doi:10.1002/anie.201905949
980 Zhou Z, Licklider LJ, Gygi SP, Reed R. 2002. Comprehensive proteomic analysis of the human spliceosome.
981 *Nature* **419**:182–185. doi:10.1038/nature01031
982

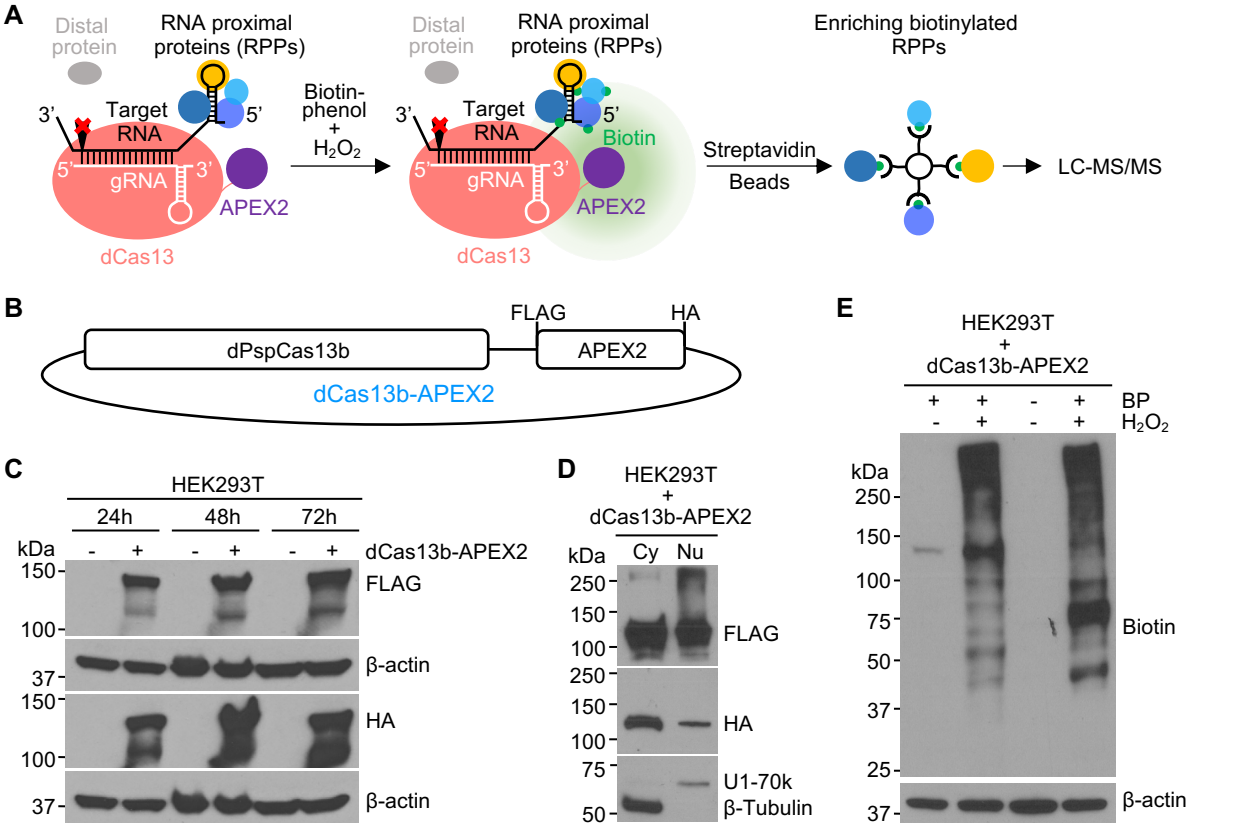
A
Distal protein
RNA proximal proteins (RPPs)
3'
Target RNA
5'
5'
gRNA
3'
APEX2
dCas13
Biotin-phenol + H_2O_2
Distal protein
RNA proximal proteins (RPPs)
3'
Target RNA
5'
Biotin
5'
gRNA
3'
APEX2
dCas13
Enriching biotinylated RPPs
Streptavidin Beads
LC-MS/MS
B
FLAG
HA
dPspCas13b
APEX2
dCas13b-APEX2
C
HEK293T
24h
48h
72h
kDa
- + - + - +
dCas13b-APEX2
150
100
FLAG
37
β-actin
150
100
HA
37
β-actin
D
HEK293T + dCas13b-APEX2
kDa
Cy Nu
250
150
100
FLAG
250
150
100
HA
75
50
U1-70k
β-Tubulin
E
HEK293T + dCas13b-APEX2
+ + - + BP
- + - + H_2O_2
kDa
250
150
100
75
50
37
25
Biotin
37
β-actin

Fig. 1

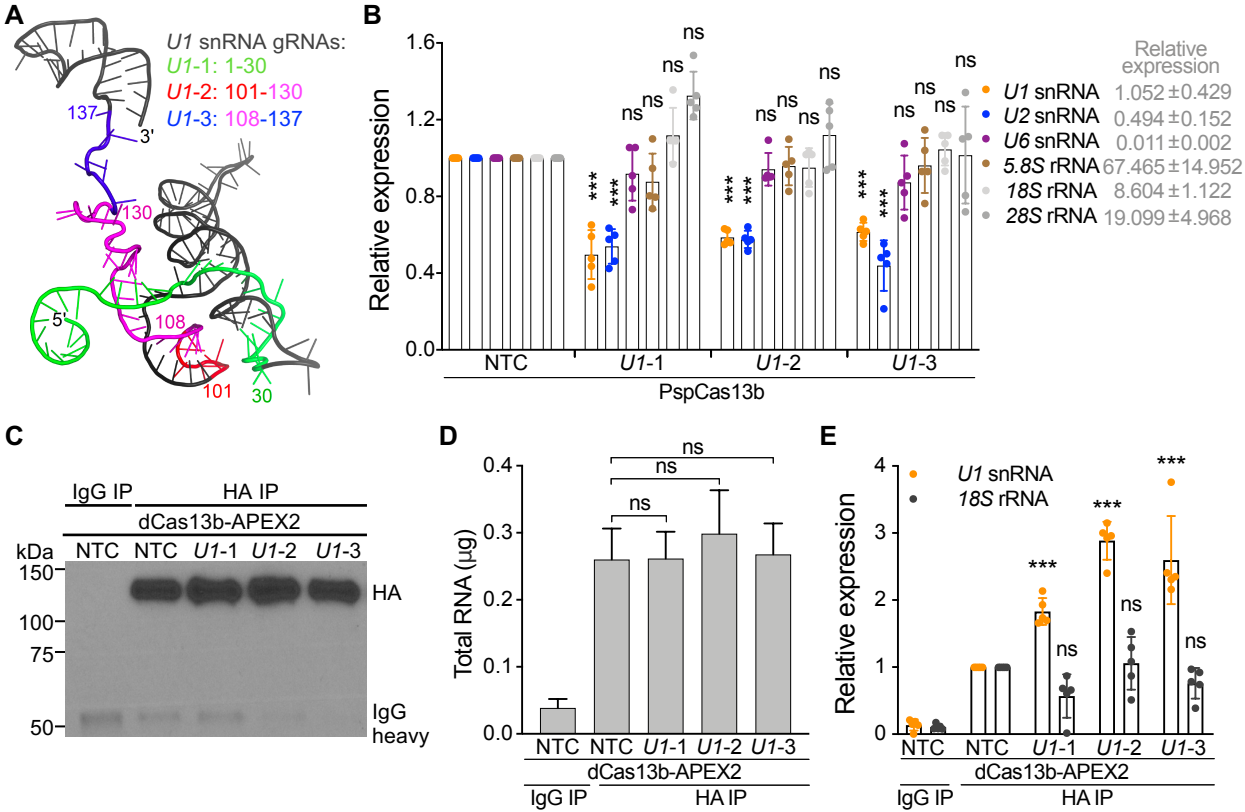
A
U1 snRNA gRNAs:
U1-1: 1-30
U1-2: 101-130
U1-3: 108-137
137
3'
130
5'
108
101
30
B
Relative expression
1.6
1.2
0.8
0.4
0.0
NTC
U1-1
U1-2
U1-3
PspCas13b
Relative expression
U1 snRNA 1.052 ±0.429
U2 snRNA 0.494 ±0.152
U6 snRNA 0.011 ±0.002
5.8S rRNA 67.465 ±14.952
18S rRNA 8.604 ±1.122
28S rRNA 19.099 ±4.968
C
IgG IP
HA IP
dCas13b-APEX2
kDa
NTC
NTC
U1-1
U1-2
U1-3
150
100
75
50
HA
IgG heavy
D
Total RNA (μg)
0.4
0.3
0.2
0.1
0.0
NTC
NTC
U1-1
U1-2
U1-3
dCas13b-APEX2
IgG IP
HA IP
E
U1 snRNA
18S rRNA
Relative expression
4
3
2
1
0
NTC
NTC
U1-1
U1-2
U1-3
dCas13b-APEX2
IgG IP
HA IP

Fig. 2

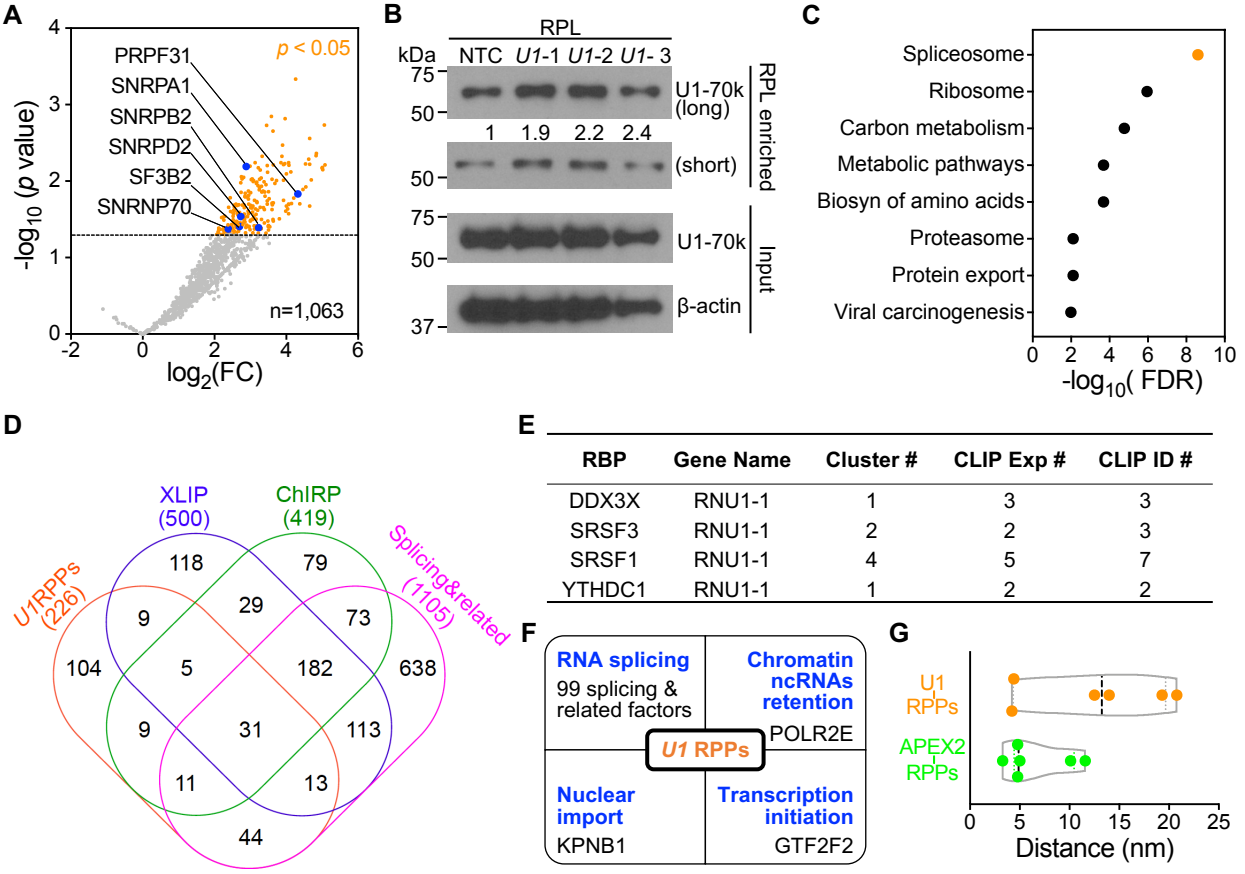

E

RBP	Gene Name	Cluster #	CLIP Exp #	CLIP ID #
DDX3X	RNU1-1	1	3	3
SRSF3	RNU1-1	2	2	3
SRSF1	RNU1-1	4	5	7
YTHDC1	RNU1-1	1	2	2

Fig. 3

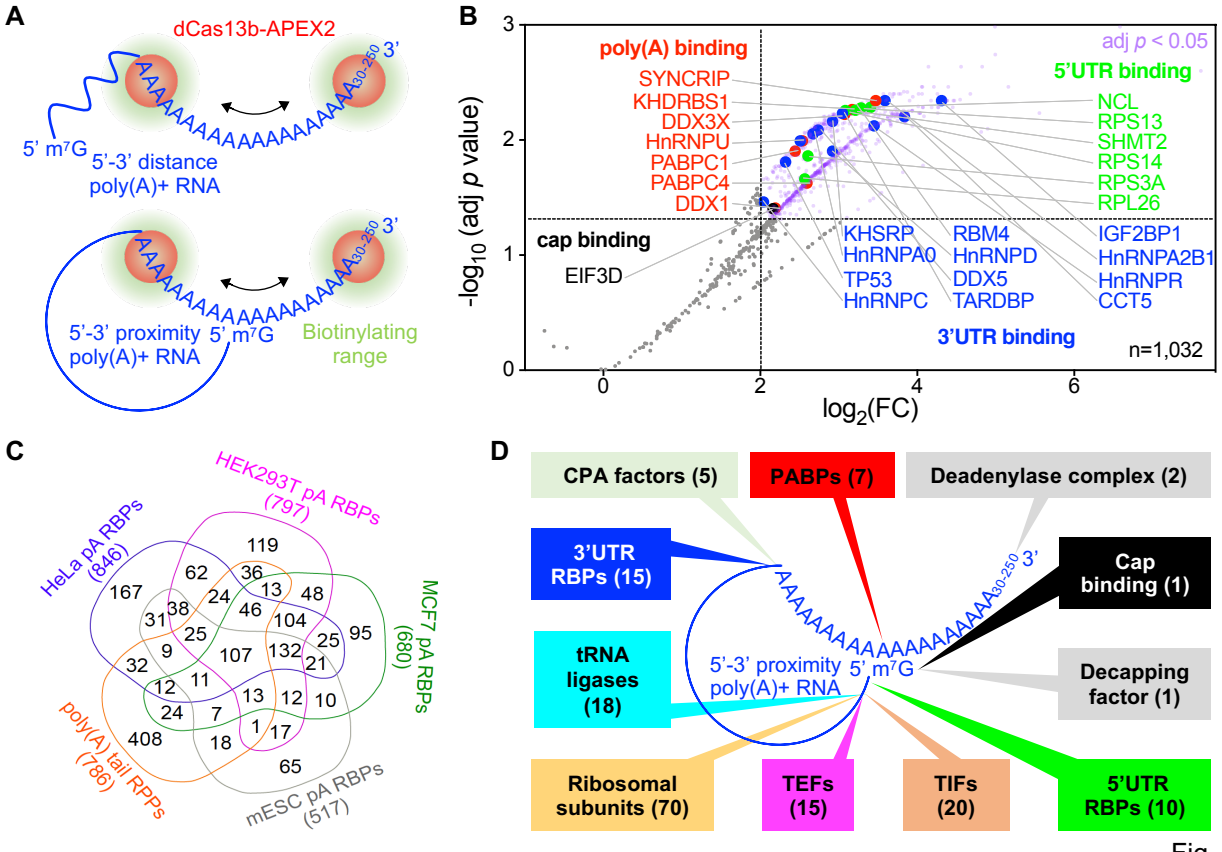
A
dCas13b-APEX2
3'
5' m7G
5'-3' distance
poly(A)+ RNA
5'-3' proximity
poly(A)+ RNA
Biotinylating
range
B
poly(A) binding
SYNCRIP
KHDRBS1
DDX3X
HnRNPU
PABPC1
PABPC4
DDX1
cap binding
EIF3D
adj p < 0.05
5'UTR binding
NCL
RPS13
SHMT2
RPS14
RPS3A
RPL26
KHSRP
HnRNPA0
TP53
HnRNPC
RBM4
HnRNPD
DDX5
TARDBP
IGF2BP1
HnRNPA2B1
HnRNPR
CCT5
3'UTR binding
n=1,032
-log10 (adj p value)
log2(FC)
C
HeLa pA RBPs (846)
HEK293T pA RBPs (797)
MCF7 pA RBPs (680)
poly(A) tail RPPs (786)
mESC pA RBPs (517)
D
CPA factors (5)
PABPs (7)
Deadenylase complex (2)
3'UTR RBPs (15)
Cap binding (1)
tRNA ligases (18)
Decapping factor (1)
Ribosomal subunits (70)
TEFs (15)
TIFs (20)
5'UTR RBPs (10)

Fig. 4

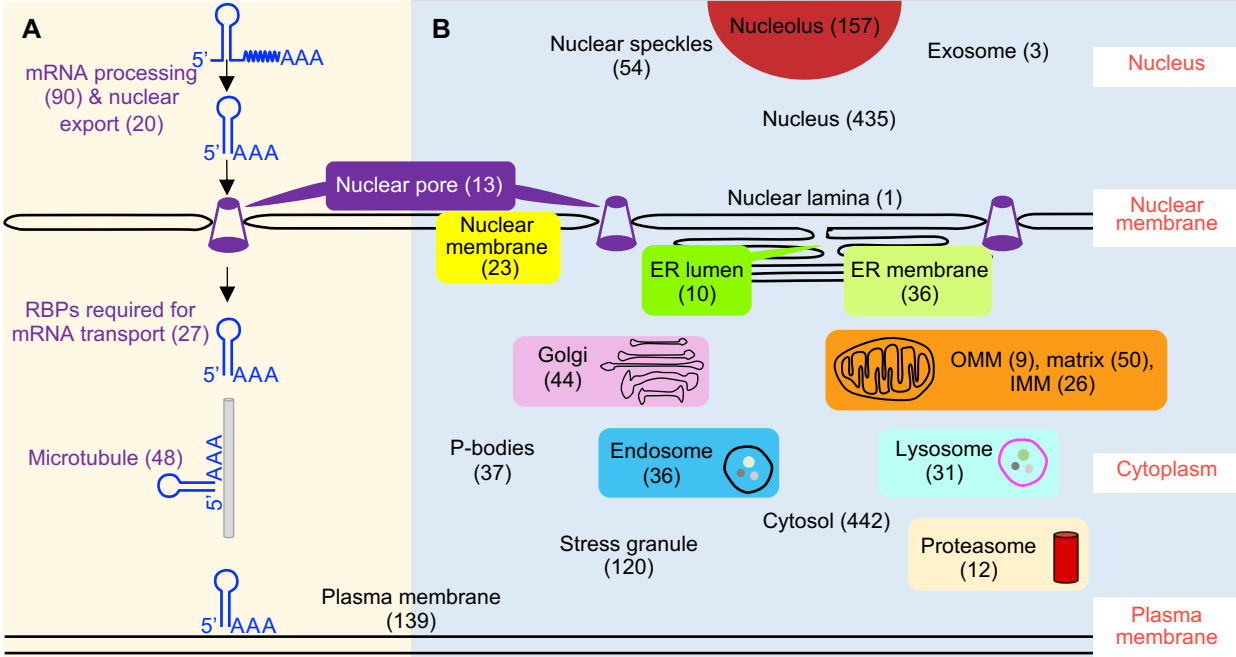
A
5'
AAA
mRNA processing (90) & nuclear export (20)
5'
AAA
Nuclear pore (13)
RBPs required for mRNA transport (27)
5'
AAA
Microtubule (48)
AAA
5'
5'
AAA
Plasma membrane (139)
B
Nucleolus (157)
Nuclear speckles (54)
Exosome (3)
Nucleus
Nucleus (435)
Nuclear lamina (1)
Nuclear membrane
Nuclear membrane (23)
ER lumen (10)
ER membrane (36)
Golgi (44)
OMM (9), matrix (50), IMM (26)
P-bodies (37)
Endosome (36)
Lysosome (31)
Cytoplasm
Cytosol (442)
Stress granule (120)
Proteasome (12)
Plasma membrane

Fig. 5

Raw western blot data

Figure 1C

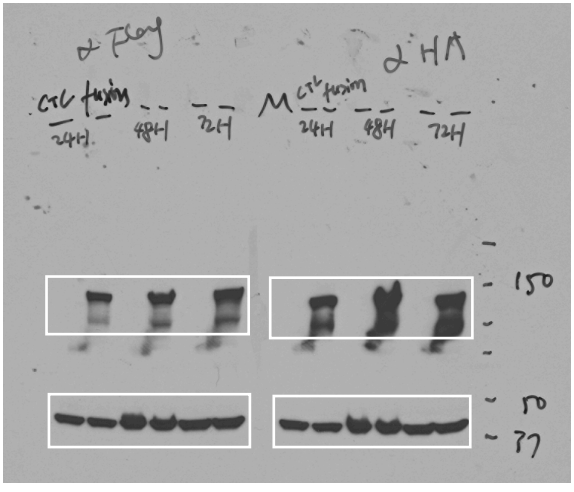

Figure 1D

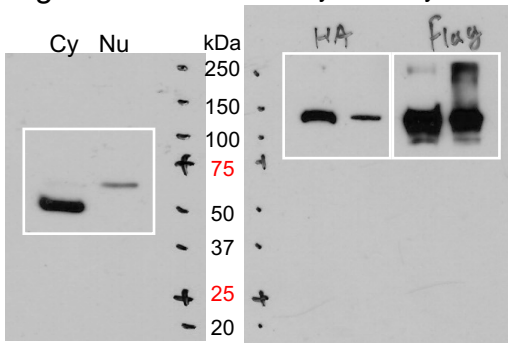

Figure 1E

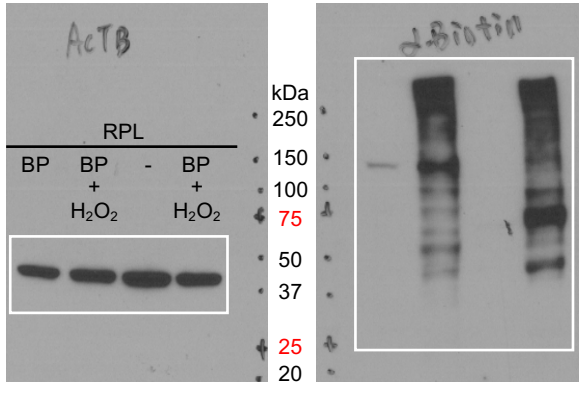

Figure 3B

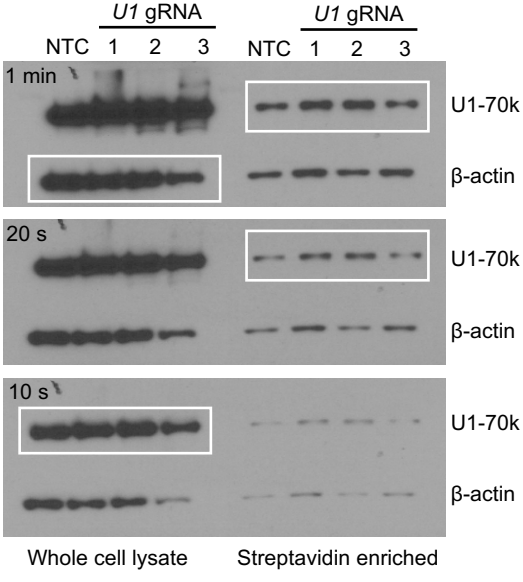
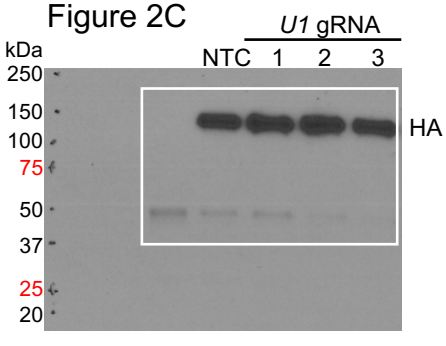
Figure 2C